Lawrence Berkeley National Laboratory
Recent Work

Title
MASS TRANSFER TO THE REAR OF AN OBJECT AT LOW REYNOLDS NUMBER FLOW

Permalink
https://escholarship.org/uc/item/2h8087k7

Author
Sih, Ping.

Publication Date
1971-05-01

eScholarship.org Powered by the California Digital Library
University of California

RECEIVED
LAWRENCE
RADIATION LABORATORY

UCRL-20509

DOCUMENTS SECTION

MASS TRANSFER TO THE REAR OF AN OBJECT AT LOW REYNOLDS NUMBER FLOW

Ping Sih
(Ph. D. Thesis)

May 1971

AEC Contract No. W-7405-eng-48

TWO-WEEK LOAN COPY

This is a Library Circulating Copy which may be borrowed for two weeks. For a personal retention copy, call Tech. Info. Division, Ext. 5545

LAWRENCE RADIATION LABORATORY
UNIVERSITY of CALIFORNIA BERKELEY

UCRL-20509

DISCLAIMER

This document was prepared as an account of work sponsored by the United States Government. While this document is believed to contain correct information, neither the United States Government nor any agency thereof, nor the Regents of the University of California, nor any of their employees, makes any warranty, express or implied, or assumes any legal responsibility for the accuracy, completeness, or usefulness of any information, apparatus, product, or process disclosed, or represents that its use would not infringe privately owned rights. Reference herein to any specific commercial product, process, or service by its trade name, trademark, manufacturer, or otherwise, does not necessarily constitute or imply its endorsement, recommendation, or favoring by the United States Government or any agency thereof, or the Regents of the University of California. The views and opinions of authors expressed herein do not necessarily state or reflect those of the United States Government or any agency thereof or the Regents of the University of California.

To my wife

Gerimae

to whom this thesis is the

fulfillment of a promise

MASS TRANSFER TO THE REAR OF OBJECTS

IN LOW REYNOLDS NUMBER FLOW

Table of Contents

ABSTRACT---------- v

INTRODUCTION---------- 1

CHAPTER I. Mass Transfer to the Rear of Sphere in Stokes Flow------ 9

A. Statement of the Problem---------- 9

B. Regions of Different Mass-Transfer Mechanisms---------- 12

C. Solution for the Region at the Rear of the Sphere---------- 26

D. Results and Discussion---------- 26

CHAPTER II. Mass Transfer to the Rear of an Object in Low Reynolds Number Flows---------- 29

A. The Axisymmetric Objects---------- 30

B. Two Dimensional, Symmetric Cylinders---------- 35

C. Conclusions---------- 41

CAHPTER III. Mass Transfer Rates to a Circular Cylinder as Predicted from the Composite Solutions and Shear Stress Distributions---- 43

CHAPTER IV. Shear Stress Measurement by a Short Electrode---------- 52

CHAPTER V. Experimental Measurement of Mass Transfer Rates to a Circular Cylinder in Low Reynolds Number Flow---------- 64

A. The Flow System---------- 64

B. Temperature Control System---------- 67

C. Electrode Construction---------- 68

D. Electrical Circuit---------- 72

E. Velocity Profile Determination---------- 77

F. Experimental Procedure---------- 78

CHAPTER VI. Experimental Results and Discussions---------- 83

ACKNOWLEDGMENTS---------- 90

APPENDIX A. Derivation of Region 3---------- 91

APPENDIX B. Electrode Construction---------- 94

APPENDIX C. Design of Damping Section---------- 95

NOMENCLATURE---------- 97

REFERENCES---------- 99

MASS TRANSFER TO THE REAR OF AN OBJECT AT LOW REYNOLDS NUMBER FLOW

Ping Sih

Inorganic Materials Research Division, Lawrence Radiation Laboratory
and Department of Chemical Engineering, University of California
Berkeley, California

ABSTRACT

Mass transfer to the rear of an object in low Reynolds number flows, where no eddies were present, was studied first theoretically. The case with Stokes flow over a sphere was analyzed in great detail. The results indicated that the same approach could be applied to a general class of practical problems; for example, flow past a symmetric two-dimensional object. In addition, the mass transfer rates to an object could be predicted providing that the shear stress distribution was known. Thus, it was not necessary to prescribe the entire flow field.

Combining the results for the rear and the front, predicted by a diffusion boundary layer as shown by Acrivos and Goddard and Levich, the mass transfer rates to the entire object could be determined.

An experiment was conducted with an electrochemical system using potassium ferricyanide, potassium ferrocyanide, a large excess of potassium nitrate as the supporting electrolyte and an electrode in the form of a circular cylinder. A flow system with a square flow tunnel (6 inches x 6 inches) was constructed. In addition, elaborate, vibration-free, constant temperature and constant flow rate systems were

provided to avoid oscillation and free convection in the flow system.

Two types of cylinder electrodes were constructed, one designed for shear stress distribution measurement, and the other, a two-electrode system for measuring the local mass transfer rate.

Reproducible data were obtained from the experimental setup with a cylinder Reynolds number of about 5. However, there were free convection effects due to the concentration difference at the electrode, contradicting the finding by Boeffard, who claimed that there was no detectable free convection at low concentrations of ferricyanide and ferrocyanide ions. Consequently, a separate research project should be performed to find a proper solution whose density does not vary with change in concentration.

INTRODUCTION

In the past few years work was done on predicting the mass transfer rates to the rear of an object by Sih and Newman [1] and Newman [2]. It focused 1) on liquid systems where the Péclet number was large, 2) on objects that were axisymmetric or two-dimensional and symmetric, and 3) on low Reynolds number flows with the absence of eddies. Schematically, such a system is shown in Figure 1. The fluid is flowing from the left to the right with uniform velocity, v_∞, and concentration, c_∞, far from the object. The object has a surface concentration c_o. Mass transfer to or from the object was investigated. Levich [3] and Acrivos and Goddard [4] investigated this system under Stokes flow condition, and they provided a solution for the front region where convection and radial diffusion were important. By the nature of their approach to the problem their answer was not valid near the rear stagnation point. To resolve this breakdown, the entire system was carefully examined by the singular perturbation method. Various regions of different transport modes were found, and the dilemma at the rear stagnation region was resolved. Newman [2] further extended the solution to include the low Reynolds number flows as well as two-dimensional objects. Basically, it was based on the fact that the velocity in the surface mass transfer regions could be approximated linearly in terms of the surface shear stress, as long as the Schmidt number was large.

In the course of these developments we became interested in studying these problems experimentally. At the same time, we found little mass transfer experiments in low Reynolds number flows. Garner and Keey [5] used benzoic acid spheres in water. Their Reynolds numbers ranged

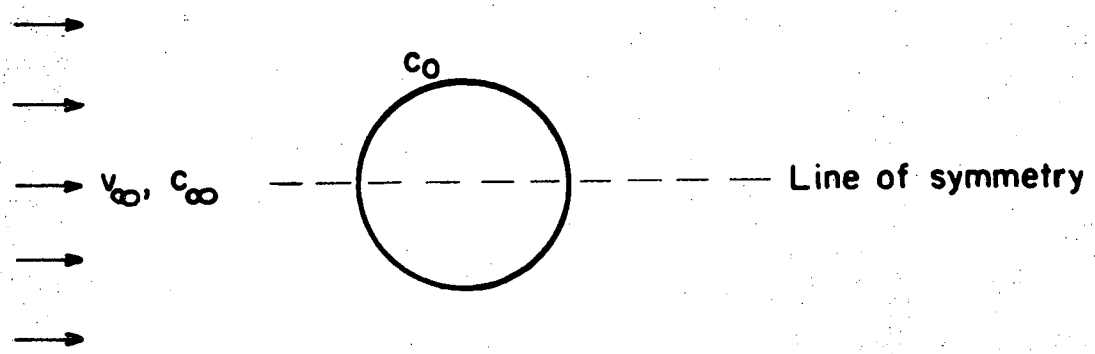

XBL712-6510

Fig. 1. Axisymmetric or 2-dimensional, symmetric object in a uniform, infinite flow field.

from 2.3 to 255. However, natural convection caused by concentration changes led to very high mass flux in the low Reynolds number flows. More recently, Dimopoulos [6] used an electrochemical system to measure the mass flux to a circular cylinder in low Reynolds number flows. The range he investigated was Reynolds numbers between 60 to 360. It was much higher than what we desired, since eddies begin to form at a Reynolds number of 5 for a circular cylinder. Furthermore, fluctuation in the mass flux at near zero flow rates was found. It was attributed to natural convection due to concentration changes. However, his apparatus was not under temperature control; hence, such fluctuations could well be caused by temperature variations.

The electrochemical system Dimopoulos used was potassium ferricyanide, potassium ferrocyanide, and a large excess of sodium hydroxide. This particular system has been used for mass transfer studies by many investigators; for example, Eisenberg [7], Bauke, Landolt and Tobias [8], Boeffard [9], Reiss and Hanratty [10], [11] Mitchell and Hanratty [12]. There are many advantages of this system:

1) There exists a long limiting current plateau in the current-potential relationship. This, at the same time, implies that the surface concentration of the reacting species is uniformly zero over the limiting current-potentials. Figure 2 is a reproduction of the current-potential curve of Eisenberg [7].

2) Activation overpotential is negligible for properly treated nickel or platinum electrodes.

3) With the presence of excess supporting electrolyte, the effect of ionic migration on the current is negligible.

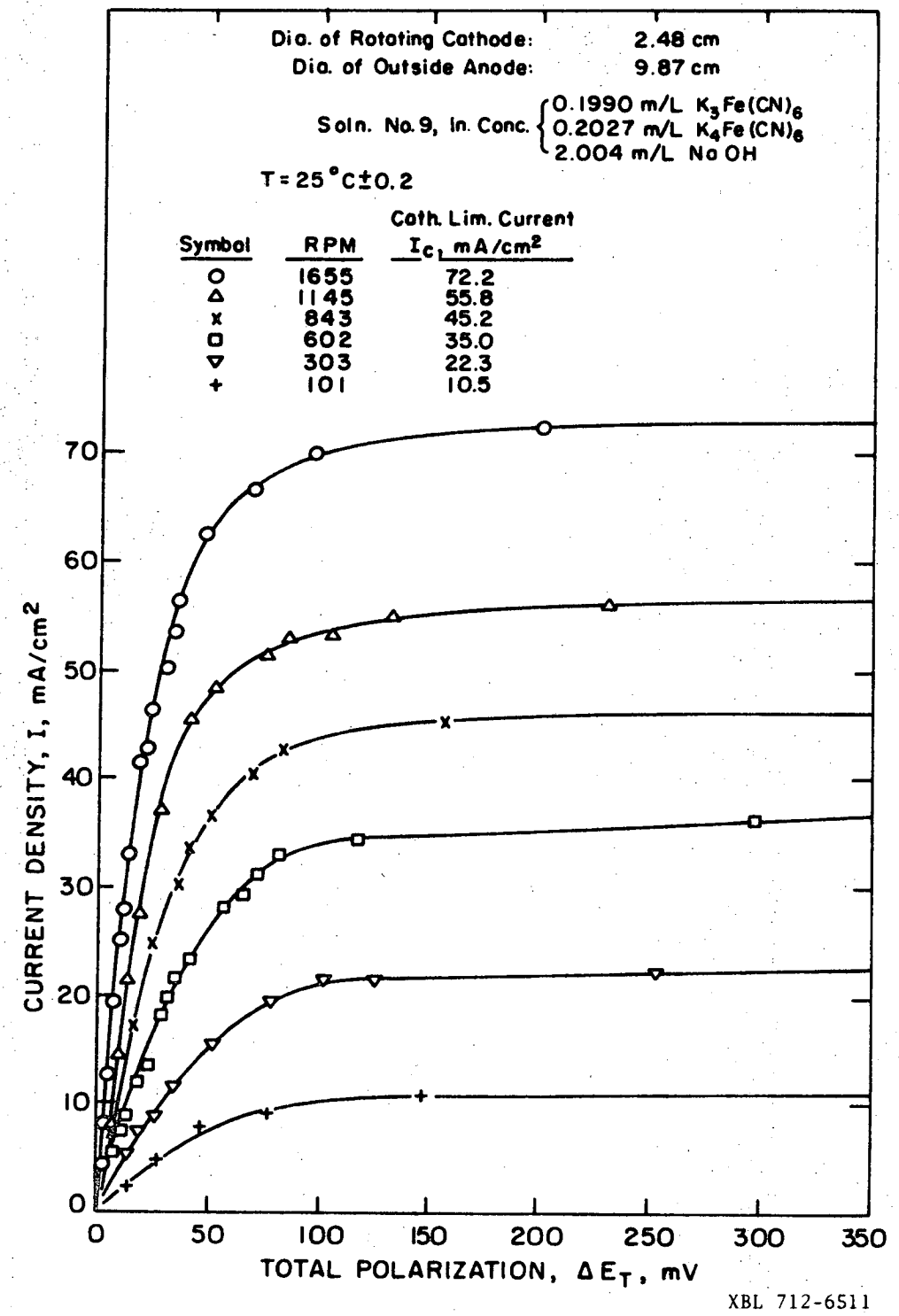

Fig. 2. Cathodic polarization curves of ferricyanide ion reduction.

4) Further, the electrochemical reaction at the electrodes is

$$Fe(CN)_6^{-3} + e^- \underset{\text{anode}}{\overset{\text{cathode}}{\rightleftharpoons}} Fe(CN)_6^{-4} \quad . \tag{1}$$

There is no dissolution or deposition of metal ions. The surface and dimensions of the electrodes are not altered during the passage of current.

In Boeffard's [9] work it was reported that at low ferricyanide and ferrocyanide concentrations (less than 0.01 M) there was no detectable natural convection effects. This, indeed, was very encouraging to us.

As mentioned above, sodium hydroxide was used as the supporting electrolyte. However, this chemical is extremely corrosive as well as harmful upon contact. For these reasons, we decided to use potassium nitrate as the supporting electrolyte. Preliminary tests were made on this system with Bauke's [8] rotating disk apparatus. No ill effects were found by this substitution. Consequently, a decision was made to use this electrochemical system, potassium ferricyanide, potassium ferrocyanide, in excess potassium nitrate, for our experiment.

Since our interest was to measure the mass flux to the rear of an object, it became necessary to set up the electrodes on the object such that the local current could be measured. This could be achieved by isolating a small section of the object as a separate electrode. By maintaining on this electrode the same potential as the rest of the object (electrode), and monitoring the current through it, the local flux could be obtained easily. Dimopoulos used such electrodes for his work.

In addition, the surface shear stress distribution over an object can be determined with the same experimental setup by means of a

differently constructed cylinder: --a small electrode embedded in an object of an electrically non-conductive material. By applying the theory developed by Lévêque [13], the current to the small electrode can be related to the local shear stress. And, Dimopoulos used this feature extensively in his work.

The specific object selected for the experiment here was a circular cylinder. There were two reasons.

1. The rear region involved a linear section. It's length could be varied until an adequate measurable current was passing the electrode. This, also, allowed us to use a very thin electrode. Incidentally, Dimopoulos sectioned out a circular area from his object as the small electrode. A simple sketch of the two-electrode, circular cylinder is shown in Figure 3.

2. Numerical results for the surface shear stress for a circular cylinder are available from the literature [14, 15, 16, 17, 18, 19, 20]. Professor Hamielec of McMaster University, Hamilton, Ontario, Canada had provided us some of his unpublished data in the range near zero Reynolds number. This is important as the mass transfer rates are governed by the shear stress distribution (see Chapter III). From these data, theoretical results can be calculated to compare with the experimental results.

The flow system used was originally designed by Thomas Atkins [21]. It contained a proto-type moving wall section for reducing wall frictions. Unfortunately, at very slow fluid velocity the equipment generated excessive vibration. Therefore, it was replaced by a simple, straight section. Figure 16 (on page 66) shows a sketch of the flow tunnel. The

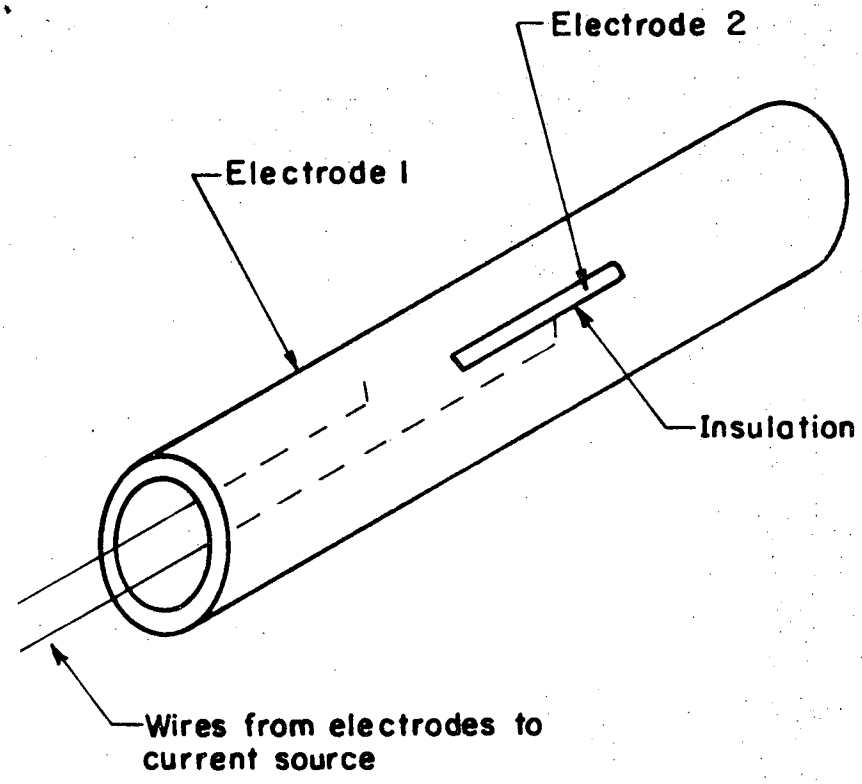

XBL712-6512

Fig. 3. A simple sketch of a two-electrode, circular cylinder.

circular cylinder was placed horizontally across the tunnel, and its mass transfer rate was measured.

To avoid natural convection due to temperature differences, the entire apparatus was placed under a strictly controlled constant temperature environment. A discussion of the temperature control system is given in Chapter V, section B.

The first part of this thesis includes the published work of Sih and Newman [1], and Newman [2]. However, more detail is included for completeness and easy comprehension.

Chapter III demonstrates how the literature shear stress data can be used with the developed theory to predict the mass transfer rates over an entire object. Chapter IV shows the derivation for measuring shear stress by a short electrode. The remaining chapters are devoted to the experimental work.

CHAPTER I: MASS TRANSFER TO THE REAR OF A SPHERE IN STOKES FLOW

This chapter is based on reference 1.

A. Statement of the Problem

The system investigated here is schematically shown in Fig. 4, where a sphere of radius R (only half is shown) is placed in a stream flowing with the velocity v_∞. The bulk concentration is c_∞, and the concentration at the surface of the sphere is c_o. When the fluid flow is so slow that $Re \to 0$, the Stokes velocity profile is applicable. The concentration difference between the bulk and the surface of the sphere will induce mass transfer between the sphere and the surrounding fluid. Our objective was to determine the local mass-transfer rates to the entire sphere.

Assuming constant physical properties, the convective diffusion equation describing this system in dimensionless form is

$$\frac{Pe}{2}\,\underline{v}^* \cdot \nabla^* \Theta = \nabla^{*2} \Theta \tag{2}$$

or in spherical coordinates

$$\frac{Pe}{2}\left(v_r^* \frac{\partial \Theta}{\partial r^*} + \frac{v_\theta^*}{r^*}\frac{\partial \Theta}{\partial \theta}\right) = \frac{\partial^2 \Theta}{\partial r^{*2}} + \frac{2}{r^*}\frac{\partial \Theta}{\partial r^*} + \frac{1}{r^{*2}}\left(\frac{\partial^2 \Theta}{\partial \theta^2} + \frac{\cos\theta}{\sin\theta}\frac{\partial \Theta}{\partial \theta}\right) \tag{3}$$

where $Pe = 2Rv_\infty/D$, the Péclet number;

D = diffusivity;

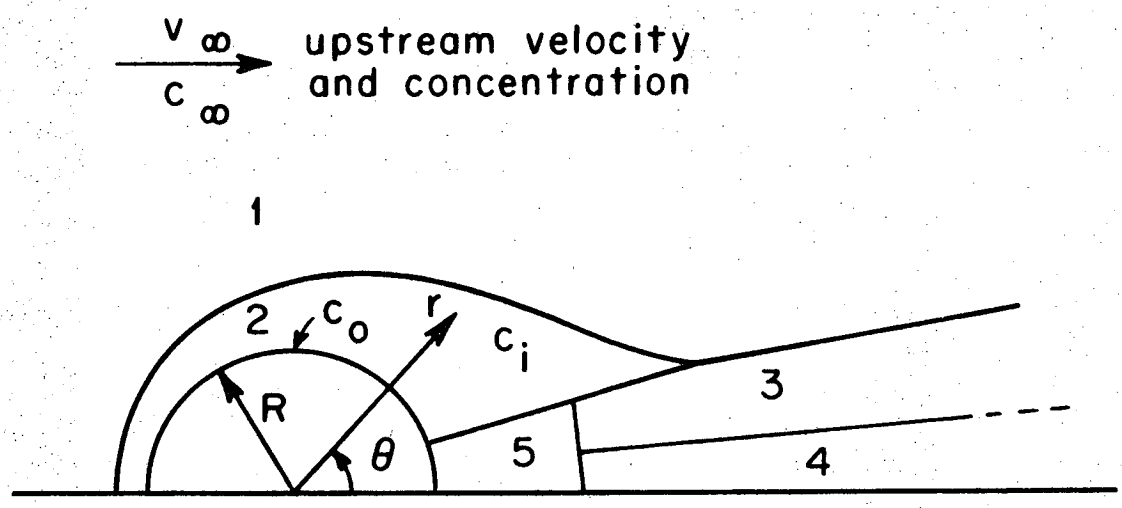

XBL671-118A

Fig. 4. Regions of dominance of different mechanisms of mass transfer, for a sphere in Stokes flow at high Péclet numbers.

$$r^* = r/R;$$

$$\Theta = (c_i - c_o)/(c_\infty - c_o);$$

and for Stokes flow

$$v_r^* = \left(1 - \frac{3}{2r^*} + \frac{1}{2r^{*3}}\right) \cos\theta \qquad (4)$$

$$v_\theta^* = -\left(1 - \frac{3}{4r^*} - \frac{1}{4r^{*3}}\right) \sin\theta. \qquad (5)$$

The boundary conditions for Equation (3) are:

1. $\Theta = 0$ at $r^* = 1$.
2. $\Theta = 1$ at $r^* = \infty$.
3. $\partial\Theta/\partial\theta = 0$ at $\theta = \pi$, the front axis.
4. $\partial\Theta/\partial\theta = 0$ at $\theta = 0$, the rear axis.

The last two boundary conditions are necessary due to symmetry.

Equation (3) does not have a simple solution. Generally boundary-layer type approximations have been used [3, 22, 4]. Such approximations are plausible in the case of liquid systems where the diffusivity is small and mass transfer takes place in a thin layer adjacent to the object. In this case diffusion along stream lines is negligible, and the important velocity is near the surface and can be approximated by a simpler form. However, the solution by such an approximation is not valid over the entire sphere since it always breaks down near the rear stagnation point. In order to correct this situation, the region where the boundary-layer approach breaks down was investigated here. Based on the method used, mass transfer to a sphere has many modes which can be

described completely by six different regions.

Briefly the method used: An approximate form of Equation (3) was first derived, then the region where the equation is valid was defined. The breakdown of this approximate equation was investigated and the region where the breakdown occurs was defined. The terms that were important in the breakdown region were subsequently determined, and a new equation appropriate to this breakdown region was derived. The process was repeated to find the next region.

B. Regions of Different Mass-Transfer Mechanisms

Region 1. Region far from the sphere.

In the bulk of the solution, the diffusion terms in Equation (3) can be neglected as $Pe \to \infty$. One has the equation

$$\underline{v}^* \cdot \nabla^* \Theta = 0 \tag{6}$$

with the solution

$$\Theta = 1. \tag{7}$$

This solution breaks down as $r^* \to 1$ since it does not satisfy the boundary condition $\Theta = 0$ at $r^* = 1$. Physically there is diffusion of material near the sphere. Also, the convective velocity is diminishing as $r^* \to 1$. In other words, near the surface the effect of convection and diffusion both become important. In fact, the velocity components can be approximated by

$$v_r^* = \left[\frac{3y^2}{2} - \frac{7y^3}{2} + 6y^4 + O(y^5)\right] \cos\theta \tag{8}$$

and

$$v_\theta^* = -\left[\frac{3y}{2} - \frac{9y^2}{4} + \frac{13y^3}{4} + O(y^4)\right] \sin\theta, \tag{9}$$

where $y = r^* - 1$.

Substitution of Equations (8) and (9) into Equation (3) yields, in the first approximation,

$$\frac{Pe}{2}\left(\frac{3y^2}{2}\cos\frac{\partial\Theta}{\partial y} - \frac{3y}{2}\sin\theta\frac{\partial\Theta}{\partial\theta}\right) = \frac{\partial^2\Theta}{\partial y^2}, \tag{10}$$

indicating that diffusion normal to the sphere will be of comparable importance to convection when y is of order $Pe^{-1/3}$. Diffusion in the tangential direction remains small and of second order importance.

Region 2. The diffusion (boundary) layer.

The above analysis of the breakdown of the solution for region 1 suggests that an appropriate variable for the region near the sphere is

$$Y = y/\varepsilon. \tag{11}$$

where $\varepsilon = (2/Pe)^{1/3}$.

The diffusion-layer equation (10) then becomes

$$\frac{3}{2}Y^2\cos\theta\frac{\partial\Theta}{\partial Y} - \frac{3}{2}Y\sin\theta\frac{\partial\Theta}{\partial\theta} = \frac{\partial^2\Theta}{\partial Y^2}, \tag{12}$$

with the boundary conditions

1. $\Theta = 0$ at $Y = 0$.
2. $\Theta = 1$ at $Y = \infty$.

3. $\partial\Theta/\partial\theta = 0$ at $\theta = \pi$.

Since the diffusion term in the θ-direction, $\partial^2\Theta/\partial\theta^2$ in equation (2), is dropped, only one boundary condition in this direction can be specified for Equation (12).

The solution for region 2 can be expressed in terms of a similarity variable

$$\eta = Y/g\ (\theta), \tag{13}$$

where

$$g(\theta) = 3^{1/3}\ [\pi - \theta + 1/2 \sin 2\theta]^{1/3}\ /\sin\theta. \tag{14}$$

The solution is

$$\Theta = \frac{1}{\Gamma(4/3)} \int_0^{\eta} e^{-\eta^3} d\eta, \tag{15}$$

where $\Gamma(4/3) = 0.89298$, the gamma function of $4/3$. The local Nusselt number Nu is

$$Nu_{bl}(\theta) = 2 \left.\frac{\partial\Theta}{\partial r^*}\right|_{r^* = 1} = \frac{2}{\varepsilon\Gamma(4/3)g(\theta)} \ . \tag{16}$$

We can examine the region of validity of this diffusion-layer solution by substituting it back into Equation (3) and examining the magnitude of the neglected terms. This gives

$$\eta^2\Theta' \left[\underline{\frac{3}{2}\ (g^3\cos\theta + g^2 g'\ \sin\theta)} - \eta g^3 \left(\frac{7}{2}\ g\cos\theta + \frac{15}{4}\ g'\ \sin\theta \right)\varepsilon + \ldots \right]$$

$$= \underline{\theta''} + 2\theta' g(1 - \eta\varepsilon g + (\eta\varepsilon g)^2 + \ldots)\varepsilon \qquad (17)$$

$$+ \left[\eta^2 g'^2 \theta'' - \eta\theta'(gg'' - 2g'^2 + \frac{\cos\theta}{\sin\theta} gg')\right] (1 - 2\eta\varepsilon g + \ldots)\varepsilon^2.$$

where the prime designates the derivative with respect to η or θ. The underlined terms, the terms of the first order of magnitude as $\varepsilon \to 0$, form the boundary-layer equation. However, as $\theta \to 0$, $g(\theta) \to O(1/\theta)$, and Equation (17) has the form

$$\frac{1}{\theta^3} - \frac{\varepsilon}{\theta^4} + \ldots = 1 + \frac{\varepsilon}{\theta} + \frac{\varepsilon^2}{\theta^4}$$

with $\eta = O(1)$. The left-hand side represents the convective terms, and the righthand side, the diffusion terms. It is easy to see that when $\theta = O(\varepsilon)$ all the terms in the velocity expansion are of the same order. In other words, as $\theta \to O(\varepsilon)$, the velocity components can no longer be approximated by expansions near the surface; consequently, the diffusion-layer approximation breaks down. Acrivos and Goddard [4] have already pointed out that this breakdown occurs as $\theta \to O(\varepsilon)$. It is physically reasonable that the complete Stokes velocity must be used because at small angles the diffusion layer becomes thick and most of it is no longer close to the sphere.

Region 3. The convective region.

The above analysis of the breakdown of the boundary-layer solution suggests that an appropriate variable for region 3 is

$$S = \theta/\varepsilon. \qquad (18)$$

Since $\eta = O(1)$ in region 2, $y = r^* - 1 = O(\varepsilon g) = O(\varepsilon/\theta) = O(1)$.

By substituting Equation (18) into Equation (3) we obtain

$$\left(1 - \frac{3}{2r^*} + \frac{1}{2r^{*3}}\right)\frac{\partial\theta}{\partial r^*} - \left(1 \frac{3}{4r^*} - \frac{1}{4r^{*3}}\right)\frac{S}{r^*}\frac{\partial\theta}{\partial S}$$

$$= \frac{\varepsilon}{r^{*2}}\left(\frac{\partial^2\theta}{\partial S^2} + \frac{1}{S}\frac{\partial\theta}{\partial S}\right) + O(\varepsilon^2). \qquad (19)$$

Thus, as $\varepsilon \to 0$, the terms to be retained are

$$\left(1 - \frac{3}{2r^*} + \frac{1}{2r^{*3}}\right)\frac{\partial\theta}{\partial r^*} - \left(1 - \frac{3}{4r^*} - \frac{1}{4r^{*3}}\right)\frac{S}{r^*}\frac{\partial\theta}{\partial S} = 0. \qquad (20)$$

In other words convection is the dominant mode of mass transfer while diffusion is relatively unimportant. The solution of this equation must match with the asymptotic form of the boundary-layer solution at $\theta = 0$, this being the standard procedure in singular-perturbation problems.

According to Equation (20), the concentration is constant along streamlines $\Theta = \Theta(\Psi)$, where from Stokes' solution the appropriate stream function for region 3 is

$$\Psi = \frac{S^2}{3^{5/3}\pi^{2/3}}\left(\frac{1}{r^*} - 3r^* + 2r^{*2}\right) . \qquad (21)$$

(Derivation is shown in Appendix A.)

The functional dependence of Θ on Ψ can be found by matching with the boundary-layer solution. Since Θ depends only on η in region 2 and only on Ψ in region 3, this functional dependence is found by matching

Ψ in region 3 to η in region 2. As $\theta \to 0$,

$$\eta = \frac{\theta y/\epsilon}{3^{1/3}\pi^{1/3}} . \tag{22}$$

On the other hand, as $r^* \to 1$,

$$\Psi \to \frac{y^2\theta^2/\epsilon^2}{3^{2/3}\pi^{2/3}} , \tag{23}$$

and consequently, in the region of matching,

$$\eta = \sqrt{\Psi} . \tag{24}$$

Hence, by the matching principle, the solution in region 3 is

$$\Theta = \frac{1}{\Gamma(4/3)} \int_0^{\sqrt{\Psi}} e^{-x^3}\, dx, \tag{25}$$

where Ψ is given by Equation (21). Note that this solution automatically matches with region 1 as $\Psi \to \infty$.

The solution (25) still does not satisfy the boundary condition $\partial\Theta/\partial\theta = 0$ at $\theta = 0$, which indicates the presence of another region very near the axis where diffusion in the θ-direction could be important. In fact, from the righthand term of Equation (19) it is apparent when $S \to \sqrt{\epsilon}$ that the diffusion terms are comparable to the convective terms on the left.

In addition, the solution of region 3 also fails as $r^* \to 1$. This is due to the reduction of the convective velocities near the surface, similar to the situation in region 2. We can put Equation (3) in the form

$$\frac{1}{\varepsilon^2}\left(Y^2\frac{\partial\theta}{\partial Y} - YS\frac{\partial\theta}{\partial S}\right) =$$

$$\frac{1}{\varepsilon^2}\frac{\partial\theta}{\partial Y^2} + \frac{1}{\varepsilon^2}\left(\frac{\partial^2\theta}{\partial S^2} + \frac{1}{S}\frac{\partial\theta}{\partial S}\right) + O\left(\frac{1}{\varepsilon}\right) + \ldots \qquad (26)$$

with $r^* - 1$ and θ simultaneously approaching $O(\varepsilon)$. We can expect yet another region right at the rear of the sphere.

Region 4. The rear-axis region.

The appropriate variables for region 4 are

$$r^* \text{ and } s, \qquad (27)$$

where $s = S / \sqrt{\varepsilon} = \theta/\varepsilon^{3/2}$.

Equation (3) then reduces to

$$\left(1 - \frac{3}{2r^*} + \frac{1}{2r^{*3}}\right)\frac{\partial\theta}{\partial r^*} - \left(1 - \frac{3}{4r^*} - \frac{1}{4r^{*3}}\right)\frac{s}{r^*}\frac{\partial\theta}{\partial s} \qquad (28)$$

$$= \frac{1}{r^{*2}}\left(\frac{\partial^2\theta}{\partial s^2} + \frac{1}{s}\frac{\partial\theta}{\partial s}\right).$$

Boundary conditions for Equation (26) are

1. $\partial\theta/\partial s = 0$ at $s = 0$.

2. $\theta \to \dfrac{\sqrt{\varepsilon}s}{\Gamma(4/3)3^{5/6}\pi^{1/3}}\left(\dfrac{1}{r^*} - 3r^* + 2r^{*2}\right)^{1/2}$ as $s \to \infty$,

   in order to match with region 3.

3. When $r^* \to 1$, as mentioned in the previous section, the velocity diminishes. A new mode of transport, indicated by Equation (26),

becomes dominant. The solution of Equation (28) must match with this new region, region 5. Note that this region, involving the tangential diffusion terms, grows thicker at greater distances from the sphere. Eventually, it blends into a sixth region, the far-wake region, where the depletion of concentration decays, first, as $1/r^*$ along the rear axis and, second, it decays exponentially in $r^*\theta^2$ in the direction normal to the axis. (See region 6 for detail).

Region 5. Region near the rear of the sphere.

From Equation (26) it is apparent that the appropriate variables are

$$Y = y/\varepsilon \text{ and } S = \theta/\varepsilon, \tag{29}$$

and Equation (3) reduces to

$$\frac{3}{2} Y^2 \frac{\partial \Theta}{\partial Y} - \frac{3}{2} YS \frac{\partial \Theta}{\partial S} = \frac{\partial^2 \Theta}{\partial Y^2} + \frac{\partial^2 \Theta}{\partial S^2} + \frac{1}{S} \frac{\partial \Theta}{\partial S} . \tag{30}$$

The boundary conditions are

1. $\Theta = 0$ at $Y = 0$.
2. $\partial\Theta/\partial S = 0$ at $S = 0$.
3. $\Theta \to \varepsilon\, YS/\Gamma(4/3)(3\pi)^{1/3}$ as $S \to \infty$,
   in order to match with the boundary-layer solution in region 2.
4. $\partial^2\Theta/\partial Y^2$ becomes negligible as $Y \to \infty$ in order to match with regions 4 and 3.

At this point, we have carried the analysis far enough to show that radial diffusion is negligible in regions 3 and 4. Consequently,

there can be no upstream propagation of effects from these regions into region 5, even though radial diffusion is not negligible in region 5 itself. This is the basis for the fourth boundary condition on Equation (28). Since we can find the asymptotic solution of Equation (28) as $Y \to \infty$, with $\partial^2\Theta/\partial Y^2 = 0$, we can express this boundary conditon in a more explicit form. Of course, this asymptotic solution is also the boundary condition for Equation (28) of region 4.

With $\partial^2\Theta/\partial Y^2 = 0$, Equation (30) can be reduced to an ordinary differential equation by a similarity variable transformation. The similarity variables are

$$\xi = S\sqrt{Y}, \quad \Theta = \varepsilon\sqrt{Y}f(\xi) \tag{31}$$

and Equation (30) becomes

$$\xi f'' + (1 + 3\xi^2/4)f' - 3\xi f/4 = 0 \tag{32}$$

with the boundary conditions

1. $f' = 0$ at $\xi = 0$.

2. $f = \xi/\Gamma(4/3)(3\pi)^{1/3}$ as $\xi \to \infty$.

The second boundary condition is required for matching with the boundary-layer solution (region 2). Equation (32) can readily be solved numerically.

This approach can be verified by simply introducing Θ of Equation (31) back into Equation (30) and comparing the terms.

For example,

$$\frac{\partial^2\Theta}{\partial Y^2} = \varepsilon(-f + \xi f' + \xi^2 f'')/4Y^{3/2}$$

and

$$\partial^2\theta/\partial s^2 = \varepsilon\, Y^{3/2} f''.$$

It is obvious that as $Y \to \infty$, $\partial^2\theta/\partial Y^2 \to 0$, and it is orders of magnitude smaller than the other terms.

To use Equation (31) as the boundary condition for Equation (28) one only needs to change the variables to yield

$$\theta \to \varepsilon^{1/2} \sqrt{(r^*-1)}\, f\,[s\sqrt{r^*-1}\,] \tag{33}$$

as $r^* \to 1$. Therefore region 4 can be solved without first solving region 5.

Since region 5 is in contact with the surface, the normal concentration gradient at the surface will yield the rate of mass transfer in the rear region. Thus, it is essential to obtain the solution of Equation (30). Boundary condition 3 on Equation (30) indicates that $\theta = 0(\varepsilon)$ in region 5. Since $y = 0(\varepsilon)$, the order of the Nusselt number in this region is $Nu = 0(\partial\theta/\partial y) = 0(1)$, in contrast to the front part of the sphere where $Nu = 0(1/\varepsilon)$, as indicated by Equation (16).

Region 6. The far wake region.

First let us examine the breakdown of region 4. As $r^* \to \infty$, Equation (28) reduces to

$$\frac{\partial\theta}{\partial r^*} - \frac{s}{r^*}\frac{\partial\theta}{\partial s} = \frac{1}{r^{*2}}\left(\frac{\partial^2\theta}{\partial s^2} + \frac{1}{s}\frac{\partial\theta}{\partial s}\right) \tag{34}$$

with boundary conditions

1. $\partial\theta/\partial s = 0$ at $s = 0$.

2. $\Theta \to \sqrt{\epsilon} s 2^{1/2} r^* / \Gamma(4/3) 3^{5/6} \pi^{1/3}$ as $s \to \infty$.

This is essentially the same as Equation (30) without the term $\partial^2\Theta/\partial Y^2$. Also, it has the similarity solution

$$\Theta = \sqrt{\epsilon}\ \sqrt{r^*}\ f(\zeta) \text{ where } \zeta = s\ \sqrt{2r^*/3} \tag{35}$$

where f is given by the solution of Equation (32) and it has the same boundary conditions. In region 4 the concentration Θ is in the order of $\sqrt{\epsilon}$. This is dictated by the boundary conditions in that region. However, as we can see from the solution above (Equation (35)) when $r^* \to O(1/\epsilon)$, $\Theta \to O(1)$. This contradiction indicates that there is another region when $r^* \to O(1/\epsilon)$. Also, the variable for region 3 $\Psi \to O(S^2 r^{*2}) \to O(\zeta^2)$ indicating region 3 is also related to region 6. Physically the concentration variation at the surface of the sphere slowly diffuses into the bulk and very far behind the sphere there exists a region where both tangential diffusion and convection are important. The above analysis suggests that an appropriate variable for region 6 is

$$\mathcal{R} = \epsilon r^*. \tag{36}$$

In order to retain terms for diffusion in the θ-direction, the appropriate variable is

$$\mathcal{S} = \theta/\epsilon^2; \tag{37}$$

then Equation (3) reduces to

$$\frac{\partial\Theta}{\partial\mathcal{R}} - \frac{\mathcal{S}}{\mathcal{R}}\frac{\partial\Theta}{\partial\mathcal{S}} = \frac{1}{\mathcal{R}^2}\left(\frac{\partial^2\Theta}{\partial\mathcal{S}^2} + \frac{1}{\mathcal{S}}\frac{\partial\Theta}{\partial\mathcal{S}}\right) \tag{38}$$

with the boundary conditions

1. $\Theta \to 1$ as $\xi \to \infty$.

2. $\partial\Theta/\partial\xi = 0$ at $\xi = 0$.

3.
$$\Theta \to \frac{1}{\Gamma(4/3)} \int_0^B \exp(-x^3)\,dx + (\sqrt{\mathcal{R}})\, f\left[\xi\sqrt{\frac{2\mathcal{R}}{3}}\right]$$

$$- \frac{\xi\mathcal{R}\sqrt{(2/3)}}{\Gamma(4/3)(3\pi)^{1/3}}$$

$$\text{as } \mathcal{R} \to 0, \text{ where } B = \frac{\xi\mathcal{R}(\sqrt{2})}{3^{5/6}\pi^{1/3}} .$$

This last boundary condition comes from matching with both region 3 and region 4 and represents the composite expansion for these two regions as $r^* \to \infty$. An interesting result of Equation (38) is its asymptotic solution as $\mathcal{R} \to \infty$. The solution can be expressed in the form of

$$\Theta = 1 - \left(\frac{K}{\mathcal{R}}\right) \exp\left(-\frac{\mathcal{R}\xi^2}{4}\right) . \tag{39}$$

The constant K is related to the total rate of mass transfer to the sphere, since the depletion of mass in the far wake must equal to that being taken up by the sphere; that is

$$-2\pi \int_0^\pi v_r(c_i - c_\infty) r^2 \sin\theta d\theta = 2\pi \int_0^\pi D \left.\frac{\partial c_i}{\partial r}\right|_{r=R} R^2 \sin\theta d\theta$$

or in dimensionless form

$$\int_0^{\pi} v_r^*(1 - \theta)r^{*2} \sin\theta d\theta = \frac{1}{Pe}\frac{1}{R^2}\int_0^{\pi} Nu(\theta)R^2 \sin\theta d\theta$$

$$= 2\frac{\overline{Nu}}{Pe} \qquad (40)$$

where $\overline{Nu}$ is the average Nusselt number. Substitution of Equation (39) into Equation (40) yields

$$K = \frac{\overline{Nu}}{(4Pe)^{1/3}} \approx 0.6245.$$

In the preceding discussion we have shown how we have proceeded logically from one region to another, examining the dominant modes of mass transfer in each region, either by observing whether the boundary conditions are satisfied or by examining the order of magnitude of terms neglected in the equation of convective diffusion. The fact that a limit of validity is found indicates the existence of an adjoining region in which different mechanisms of mass transfer are important. Although specific solutions for all the regions are not sought, a complete picture of the transport process involved as well as the concentration distributions becomes very clear. Table I is a summary of the mechanisms and concentration magnitudes.

Table I. Transport mechanisms and the upper limits of concentration magnitudes

Regions	Mechanism	Upper limits of concentration magnitudes
1.	convection	$0(1)$
2.	convection and diffusion, normal to the surface	$0(1)$
3.	convection	$0(1)$
4.	convection and diffusion, tangential to the surface	$0(\sqrt{\varepsilon})$
5.	convection and diffusion in all directions	$0(\varepsilon)$
6.	convection and diffusion, tangential to the surface	$0(1)$

C. Solution for the Region at the Rear of the Sphere

In the preceding discussion the mass transfer processes for the entire flow field were shown. However, to predict the mass transfer rate to a sphere only the solutions for regions 2 and 5 are required since the these are the two regions that are in direct contact with the sphere. The solution for region 2 is given by Equation (15). However, an analytical solution of Equation (30) for region 5 is not possible. Therefore, a numerical solution was sought. The problem posed was solved by finite-difference methods using successive over-relaxation on a high-speed digital computer. The results are shown in the next section.

D. Results and Discussion

From the calculated concentration distribution in the rear-stagnation region, the mass transfer rate along the surface can be obtained from the normal gradient at the surface. The local Nusselt number $Nu_r = 2\ \partial\Theta/\partial r^* \big| r^* = 1$ can then be calculated. The subscript r denotes the solution for the rear region. The result is shown in Figure 5. Also shown in Figure 2 is the local Nusselt number Nu_{bl} predicted by the boundary-layer solution. It is clear, as one would expect, that there is a large difference at small angles, and yet the solution for region 5 blends into the boundary-layer solution at larger angles.

At the rear stagnation point, S = 0, the local Nusselt number is $Nu_r = 1.192$. This is less than the Nusselt number (Nu = 2) for the diffusion from a sphere into a stagnant medium. The reason, obviously, is that the convection of depleted solution into the rear region decreases the concentration gradient at the rear.

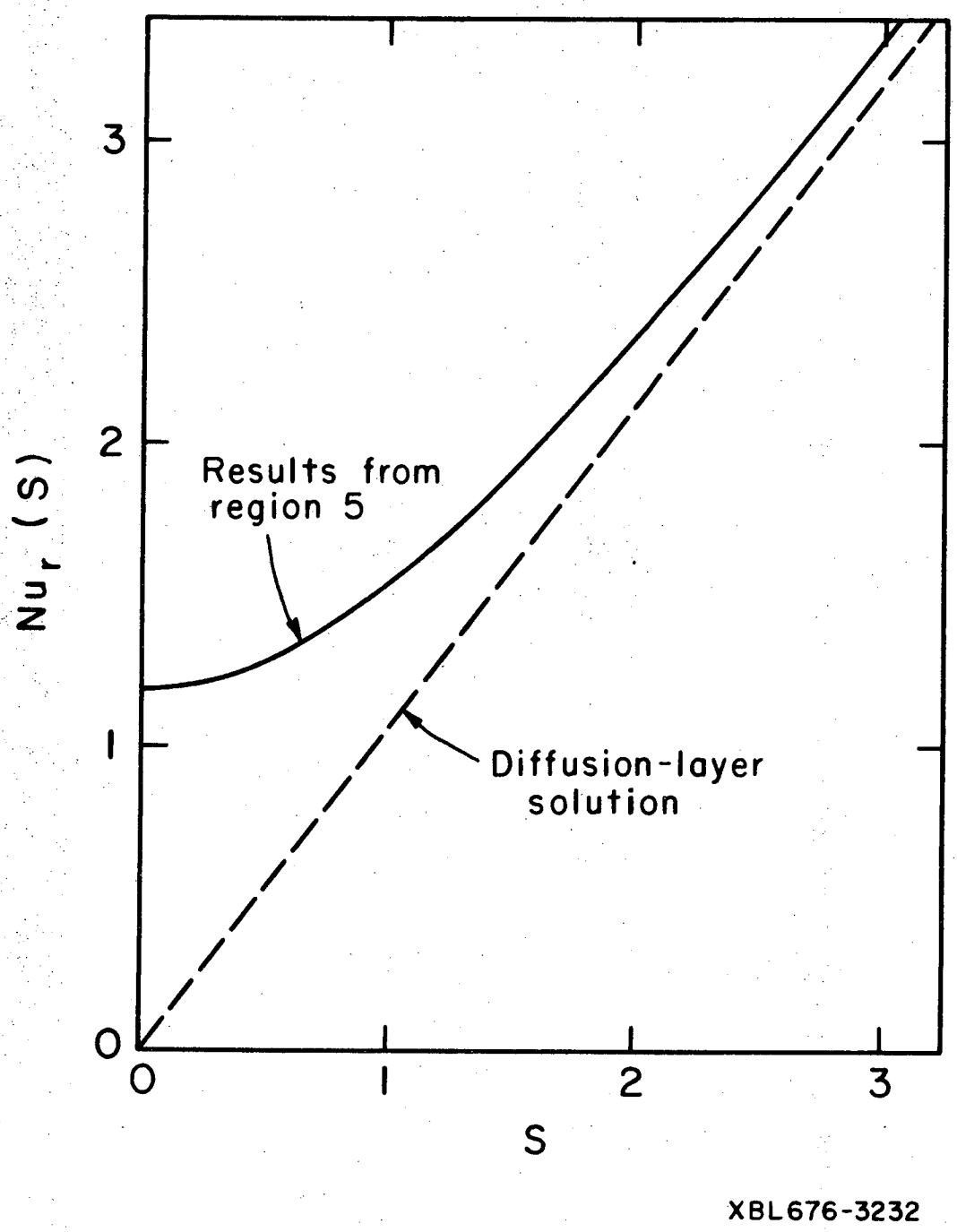

Fig. 5. Local Nusselt number in the region near the rear of the sphere.

In order to obtain the mass-transfer rate for the entire sphere, it is necessary to form a composite solution, with the boundary-layer solution as the outer solution and the solution for the rear region as the inner solution. Mathematically, the composite solution for the local Nusselt number can be written as

$$Nu(\theta) = Nu_{bl}(\theta) + Nu_{r}(S) - 2\theta/\varepsilon\Gamma(4/3)(3\pi)^{1/3}, \qquad (41)$$

where the subscript bl denotes the boundary-layer solution. The last term is the inner limit of the boundary-layer solution, which is the same as the outer limit of the solution for region 5.

Acrivos and Goddard [4] have obtained the asymptotic average N Nusselt number for $Pe \to \infty$, and $Re \to 0$, as

$$\overline{Nu} = Pe^{1/3}\,[0.9914 + 0.922\,Pe^{-1/3} + O(Re) + O(Pe^{2/3})], \qquad (42)$$

and they also have suggested that the contribution of the rear stagnation region to $\overline{Nu}$ is $O(Pe^{-1/3})$, although it actually is of the order $Pe^{-2/3}$. Therefore, if one wants to include the contribution to $\overline{Nu}$ of the rear stagnation region, one should also carry out two more higher order approximations in Acrivos and Goddard's analysis for the diffusion layer.

CHAPTER II: MASS TRANSFER TO THE REAR OF AN OBJECT IN LOW REYNOLDS NUMBER FLOWS

This chapter is based on reference 2.

In Chapter I we have shown how to remedy the breakdown of a boundary-layer solution with a specific example. Note that Equations (12) and (30) for regions 2 and 4, respectively, have the same velocity components

$$v_\theta \alpha y \text{ and } v_r \alpha y^2.$$

This should not be surprising since both regions are very close to the surface and the same velocity approximation is applicable. In a more general form the velocity components can be expressed in terms of the surface shear stress; that is,

$$v_x = y\beta(x)$$

$$v_y = -(1/2)y^2 \frac{(P(x)\beta(x))'}{P(x)} \tag{43}$$

where: $\beta(x) = \left.\frac{\partial v_x}{\partial y}\right|_{y=0}$

x = the distance measured along the surface from the front

P(x) = the normal distance of the surface from the axis of symmetry.

Prime denotes the first order derivative with respect to x. Note that Equation (2) is written in terms of a general form for an axisymmetric body. Thus, when the shear stress data are available, it becomes possible to estimate the velocity components and consequently to calculate the rate of mass transfer to an object, although the body is

limited in shape to ones with rounded back sides as shown in Figure 6.

In the next two sections we shall formulate the mass transfer equations and solutions for the axisymmetric objects (extension of the sphere problem) and the two-dimensional, symmetric cylinders.

A. The Axisymmetric Objects

In terms of x and y, the diffusion equation becomes

$$v_x \frac{\partial \Theta}{\partial x} + v_y \frac{\partial \Theta}{\partial y} = D\left(\frac{\partial^2 \Theta}{\partial y^2} + \frac{1}{P}\frac{\partial}{\partial x} P \frac{\partial \Theta}{\partial x}\right), \tag{44}$$

this equation holding very near to the surface. Note, Equation (44) is not dimensionless because there is no characteristic length such as the radius of a sphere.

For the diffusion layer, the last term is negligible. After substituting Equation (43) into Equation (44), the resultant equation can be solved in the same manner as Equation (12) of region 2. The solution is still

$$\Theta = \frac{1}{\Gamma(4/3)} \int_0^{\eta} e^{-\eta^3} dy \tag{15}$$

but

$$\eta = \frac{y\sqrt{P\beta}}{\left[9D \int_0^x P \sqrt{P\beta}\, d\bar{x}\right]^{1/3}} \tag{45}$$

As has been shown in Chapter I, the rear region is very small; therefore, it should be possible to approximate further the velocity profiles in this region by assuming a linear relationship such as

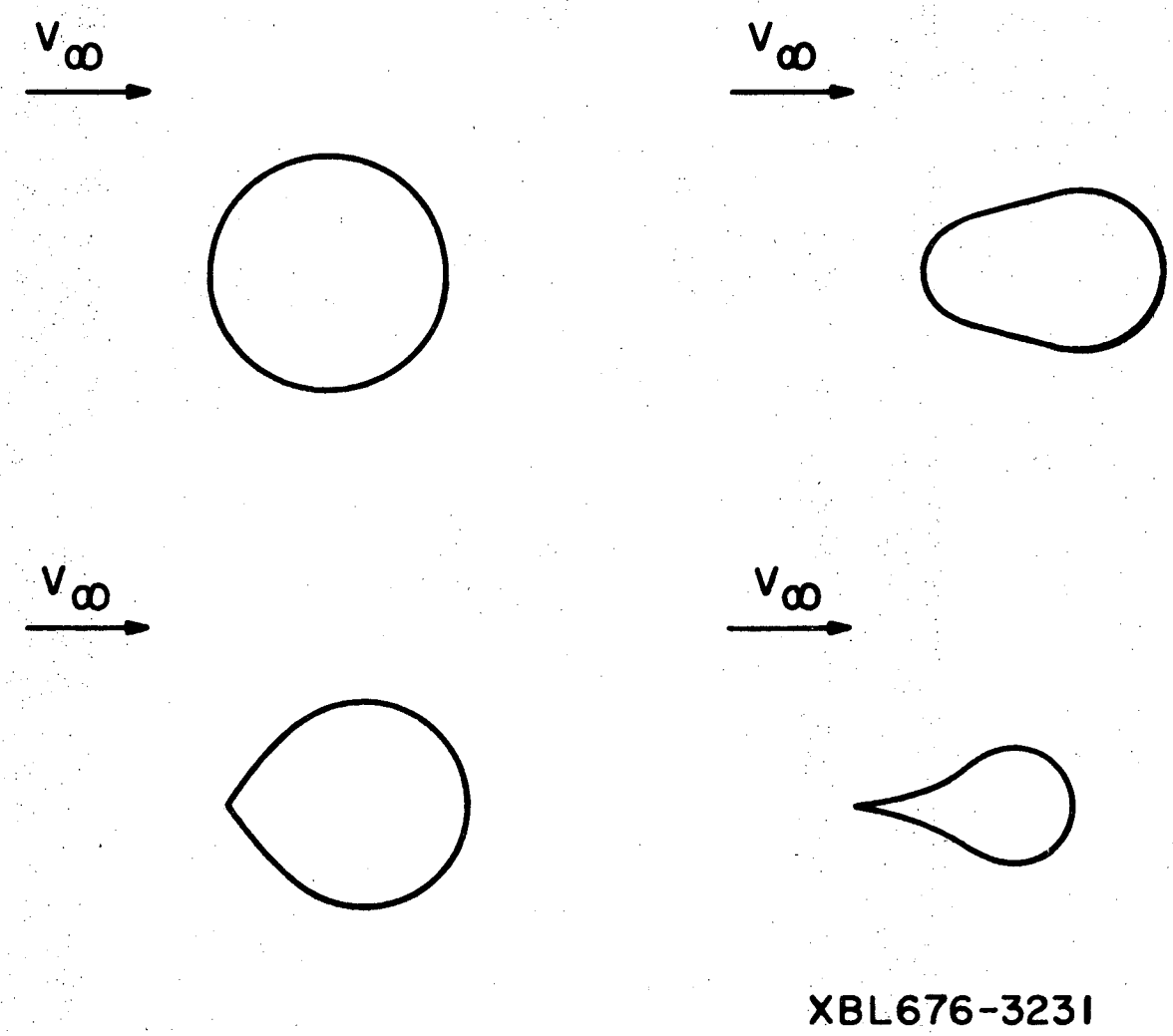

Fig. 6. Symmetric cylinders or axisymmetric bodies with rounded back sides.

$$\beta = A(x_o - x) \text{ as } x \to x_o \tag{46}$$

where x_o is the value of x at the rear stagnation point and A is a constant. Equation (46) implies that the shear stress diminishes linearly with respect to x. Thus, the convective diffusion equation becomes

$$APy \frac{\partial \Theta}{\partial x} + Ay^2 \frac{\partial \Theta}{\partial y} = D\left(\frac{\partial^2 \Theta}{\partial y^2} + \frac{1}{P}\frac{\partial}{\partial x} P \frac{\partial \Theta}{\partial x}\right), \tag{47}$$

Since for our case $P = x_o - x$ (see Figure 6). If Equation (30) of region 5 can be generalized to other objects, we must show that Equation (47) can be reduced to the same form and with appropriate boundary conditions. This is achieved by the following transformation:

$$Y = y(2A/3D)^{1/3}, \quad S = P(2A/3D)^{1/3} = (x_o - x)(2A/3D)^{1/3}. \tag{48}$$

In the coordinates Y and S, the similarity variable η of the diffusion-layer solution is

$$\eta = \frac{y\sqrt{P\beta}}{\left[9D \int_o^{x_o} P\sqrt{P\beta}\, dx\right]^{1/3}} = \frac{YSD^{1/3}}{\left[4\sqrt{A} \int_o^{x_o} P\sqrt{P\beta}\, dx\right]^{1/3}} . \tag{49}$$

Consequently, in order to match with the diffusion-layer solution, the solution in the rear region must satisfy the condition

$$\Theta \to \frac{\eta}{\Gamma(4/3)} = \frac{YS}{\Gamma(4/3)} \frac{D^{1/3}}{\left[4\sqrt{A} \int_o^{x_o} P\sqrt{P\beta}\, dx\right]^{1/3}} \tag{50}$$

as $S \to \infty$.

With a new dimensionless concentration

$$\overline{\Theta} = \Theta \frac{\Gamma(4/3)}{D^{1/3}} \left[4\sqrt{A} \int_0^{x_o} P\sqrt{P\beta}\, dx\right]^{1/3} , \tag{51}$$

the problem becomes independent of the conditions on the front part of the body. Now Θ satisfies

$$\frac{3}{2} Y^2 \frac{\partial \overline{\Theta}}{\partial Y} - \frac{3}{2} YS \frac{\partial \overline{\Theta}}{\partial S} = \frac{\partial^2 \overline{\Theta}}{\partial Y^2} + \frac{\partial^2 \overline{\Theta}}{\partial S^2} + \frac{1}{S} \frac{\partial \overline{\Theta}}{\partial S} , \tag{52}$$

subject to the boundary conditions

1. $\overline{\Theta} = 0$ at $Y = 0$, on the solid surface.
2. $\partial\overline{\Theta}/\partial S = 0$ at $S = 0$, on the rear axis.
3. $\overline{\Theta} \to YS$ as $S \to \infty$, in order to match with the diffusion-layer solution.
4. As $Y \to \infty$, the term $\partial^2\overline{\Theta}/\partial Y^2$ should become negligible.

Equation (52) is the same as Equation (30) except boundary condition 3, where the concentration is different by a constant factor. However, except for its magnitude, such a constant factor does not affect the concentration profile or its gradient. Hence, the solution for the sphere problem remains applicable. Figure 5 is replotted in Figure 7 in terms of $\partial\overline{\Theta}/\partial Y$ at $Y = 0$ in order to be useful for the wider range of problems treated in this section.

For large S. the surface concentration gradient reaches an asymptote

$$\partial\overline{\Theta}/\partial Y\Big|_{Y=0} \to S + \frac{0.406}{S} \quad \text{as } S \to \infty \tag{53}$$

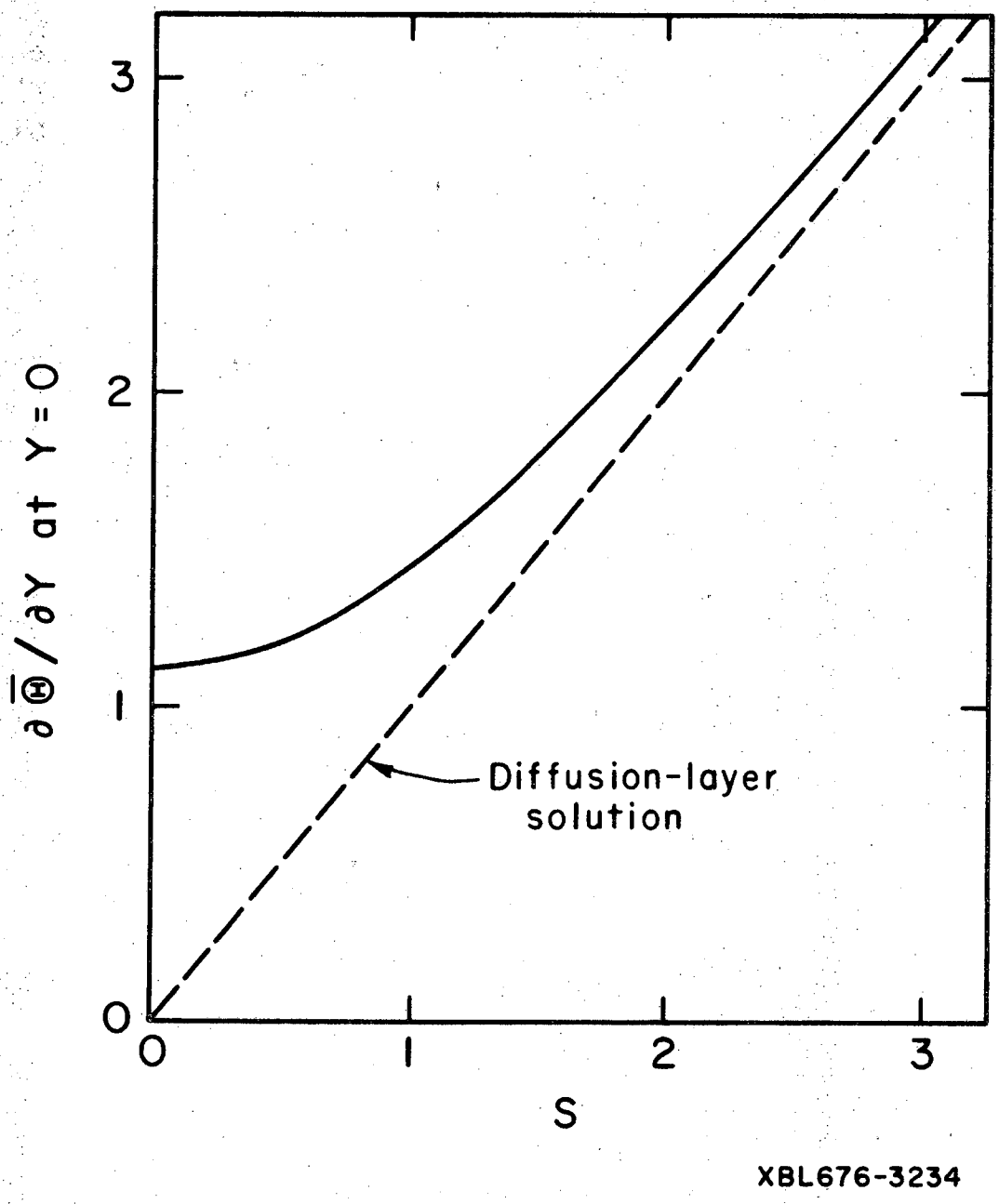

Fig. 7. Rate of mass transfer near the rear of a bluff axisymmetric body at large Schmidt numbers.

while at the rear itself the value is 1.124.

B. Two Dimensional, Symmetric Cylinders

For a two-dimensional, symmetric cylinder under the same physical conditions -- high Schmidt number and low Reynolds number flows -- the Lighthill transformation [23] provides a similarity solution for the concentration profile in the diffusion layer, as pointed out by Acrivos [24]. In fact, the velocity components used are

$$v_x = y\beta(x)$$

$$\text{and} \quad v_x = -(1/2)y^2\beta'(x) \tag{54}$$

and the solution in the diffusion layer is

$$\Theta = \frac{1}{\Gamma(4/3)} \int_0^{\eta} e^{-\eta^3}\, d\eta, \tag{55}$$

the same as Equation (15). However, here,

$$\eta = \frac{y\sqrt{\beta}}{\left[9D \int_0^x \sqrt{\beta}\, dx\right]^{1/3}} \tag{56}$$

x, again, is measured along the surface from the front and y is the normal distance from the surface.

Since the Lighthill method is based upon the same type of arguments as that of the boundary-layer method, it also breaks down at the rear of an object. However without going into as great detail as in the sphere case we should suspect that the region of interest at the rear is small in both the x and y directions. Consequently, x and y are essentially

Cartesian coordinates in this region. The convective diffusion equation thus can be written as

$$v_x \frac{\partial \Theta}{\partial x} + v_y \frac{\partial \Theta}{\partial y} = D\left(\frac{\partial^2 \Theta}{\partial x^2} + \frac{\partial^2 \Theta}{\partial y^2}\right) . \tag{57}$$

By substituting the velocity approximations and letting $B \to A(x_o - x)$ as $x \to x_o$, Equation (57) is reduced to

$$Ay(x_o - x) \frac{\partial \Theta}{\partial x} + \frac{1}{2} Ay^2 \frac{\partial \Theta}{\partial y} = D\left(\frac{\partial^2 \Theta}{\partial x^2} + \frac{\partial^2 \Theta}{\partial y^2}\right) . \tag{58}$$

The diffusion coefficient and the constant A can be made to disappear by stretching the coordinates:

$$X = (x_o - x)(A/D)^{1/3}, \quad Y = y(A/D)^{1/3} , \tag{59}$$

so that Θ satisfies the equation

$$\frac{1}{2} Y^2 \frac{\partial \Theta}{\partial Y} - YX \frac{\partial \Theta}{\partial X} = \frac{\partial^2 \Theta}{\partial X^2} + \frac{\partial^2 \Theta}{\partial Y^2} . \tag{60}$$

Near the rear region the similarity variable η of the diffusion layer can be expressed in these coordinates in the form

$$\eta = \frac{y\sqrt{\beta(x)}}{\left[9D \int_o^{x_o - x(D/A)^{1/3}} \sqrt{\beta}\, dx\right]^{1/3}} \approx \frac{y\sqrt{A(x_o - x)}}{\left[9D \int_o^{x_o} \sqrt{\beta}\, dx\right]^{1/3}} = Y\sqrt{X}\left[\frac{\sqrt{D}}{9 \int_o^{x_o} \sqrt{\beta}\, dx}\right]^{1/3} , \tag{61}$$

which is small because the diffusion coefficient is small. Hence, in order to match the solution in the rear region with the diffusion-layer solution, we must have

$$\Theta \to \frac{Y\sqrt{X}}{\Gamma(4/3)} \left[\frac{\sqrt{D}}{9 \int_0^{x_o} \sqrt{\beta}\, dx} \right]^{1/3} \quad \text{as } X \to \infty. \tag{62}$$

The problem in the rear region can finally now be made independent of by stretching the concentration. Let

$$\overline{\Theta} = \Theta\, \Gamma(4/3) \left[\frac{9}{\sqrt{D}} \int_0^{x_o} \sqrt{\beta}\, dx \right]^{1/3} . \tag{63}$$

This will also make the problem for $\overline{\Theta}$ independent of the Reynolds number and of the geometry of the front part of the cylinder.

The diffusion equation now becomes

$$\frac{1}{2} Y^2 \frac{\partial \overline{\Theta}}{\partial Y} - YX \frac{\partial \overline{\Theta}}{\partial X} = \frac{\partial^2 \overline{\Theta}}{\partial X^2} + \frac{\partial^2 \overline{\Theta}}{\partial Y^2} , \tag{64}$$

with the boundary conditions

1. $\overline{\Theta} = 0$ at $Y = 0$, on the solid surface.
2. $\partial\overline{\Theta}/\partial X = 0$ at $X = 0$, on the plane of symmetry.
3. $\overline{\Theta} \to Y\sqrt{X}$ as $X \to \infty$, in order to match with the diffusion-layer solution.
4. As $Y \to \infty$, we suspect that $\partial^2\overline{\Theta}/\partial Y^2$ should become negligible, in order to match with regions downstream where diffusion in the direction normal to the surface should be negligible.

The last boundary condition can be stated more explicitly by finding the asymptotic solution as $Y \to \infty$. Then $\overline{\Theta}$ should satisfy the equation

$$\frac{1}{2} Y^2 \frac{\partial \overline{\Theta}}{\partial Y} - YX \frac{\partial \overline{\Theta}}{\partial X} = \frac{\partial^2 \overline{\Theta}}{\partial X^2} \tag{65}$$

with the solution

$$\overline{\Theta} \to Y^{3/4} F(\xi) \text{ where } \xi = X\sqrt{Y} \tag{66}$$

and where F satisfies the ordinary differential equation

$$F'' + \frac{3}{4} \xi F' - \frac{3}{8} F = 0 \tag{67}$$

with the boundary conditions

$$F' = 0 \text{ at } \xi = 0 \text{ and } F \to \sqrt{\xi} \text{ as } \xi \to \infty.$$

The problem posed in Equation (64) was also solved by finite-difference methods using successive overrelaxation on a high-speed digital computer, the method being similar to that used for mass transfer to the rear of a sphere. The rate of mass transfer to the cylinder in the rear region can be calculated from the values of $\partial\overline{\Theta}/\partial Y$ at $Y = 0$, which are plotted in Figure 8. The value at the rear itself is 0.819. From these values and the diffusion-layer solution, a composite expansion for the mass-transfer rate can be constructed. The local Nusselt number is of order $Sc^{1/6}$ near the rear of the cylinder.

It may be pointed out that the solution in the rear region approaches the diffusion-layer solution from below rather than from above

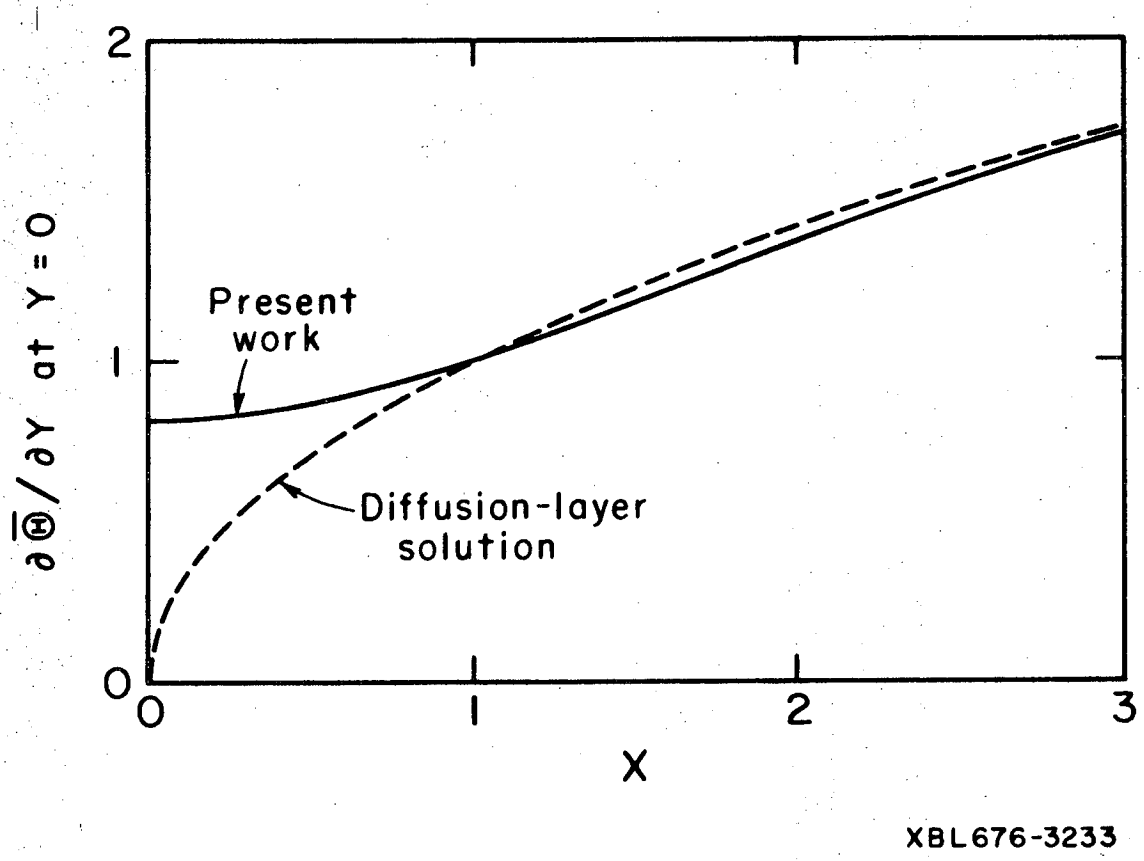

Fig. 8. Rate of mass transfer near the rear of a bluff two-dimensional body at large Schmidt numbers.

as $X \to \infty$. That this is really the case can be verified by obtaining the asymptotic solution for $\overline{\Theta}$ as $X \to \infty$. Let

$$\overline{\Theta} = Y\sqrt{X} + T. \tag{68}$$

Substitution into Equation (64) gives a differential equation for T:

$$\frac{1}{2} Y^2 \frac{\partial T}{\partial Y} - YX \frac{\partial T}{\partial X} = - \frac{Y}{4X^{3/2}} + \frac{\partial^2 T}{\partial X^2} + \frac{\partial^2 T}{\partial Y^2} . \tag{69}$$

The term $- Y/4X^{3/2}$ acts as a negative source in this equation. By neglecting the term $\partial^2 T/\partial X^2$ as $X \to \infty$, one obtains the solution for T as $X \to \infty$:

$$T = G(Y)/X^{3/2} , \tag{70}$$

where G satisfies the ordinary differential equation

$$4G'' = Y + 2Y^2 G' + 6YG \tag{71}$$

and the boundary conditions

$$G = 0 \text{ at } Y = 0 \quad \text{and } G \to -1/6 \text{ as } Y \to \infty.$$

Thus the concentration derivative can be expressed for large X as

$$\left.\frac{\partial \overline{\Theta}}{\partial Y}\right|_{Y=0} \to \sqrt{X} + \frac{G'(0)}{X^{3/2}} = \sqrt{X} - \frac{0.1242}{X^{3/2}} \text{ as } X \to \infty. \tag{72}$$

Here $\sqrt{X}$ represents the diffusion-layer solution as plotted in Figure 8 and the correction term $G'(0)/X^{3/2}$ is negative.

C. Conclusion

From the preceding discussions it is apparent that the mass transfer rate at the rear is orders of magnitude smaller than the rates in the front, and its contribution to the average Nusselt number is negligible. However, the method used shows a means to remedy the breakdown of the diffusion layer approach. Like pieces of a puzzle properly matched, examination from region to region uncovers the various mechanisms of mass transfer, thus forming a complete picture which describes the entire transport process. In addition when one sorts high order contributions to the average Nusselt number, such as the work done by Acrivos and Goddard, [4] one must eventually take into account the singular behavior at the rear stagnation point. The work done here provides the necessary information for that purpose.

Table II shows the Schmidt number dependence of the Nusselt number for both two-dimensional and axisymmetric cases.

Table II. Schmidt-number dependence of the Nusselt number at high Schmidt numbers.

	Two-dimensional problem	Axisymmetric problem
order of local Nusselt number in the rear region	$O(Sc^{1/6})$	$O(1)$
order of contribution of rear region to the average Nusselt number	$O(Sc^{-1/6})$	$O(Sc^{-2/3})$
order of average Nusselt number	$O(Sc^{1/3})$	$O(Sc^{1/3})$

CHAPTER III: MASS TRANSFER RATES TO A CIRCULAR CYLINDER AS PREDICTED FROM THE COMPOSITE SOLUTION AND SHEAR STRESS DISTRIBUTIONS

The surface vorticity distribution over a circular cylinder, or sphere, in low Reynolds number flow is readily available in the literature. For example, Jenson [25], Hamielec, Hoffman, and Ross [26] calculated the surface vorticity for a sphere, while Sih [27], Southwell and Squire [28], Apelt [14], Allen and Southwell [15], Thom [16], Takami and Keller [17], Jain and Rao [18], Dennis and Chang [19] and Kawaguti [20] studied the case for a circular cylinder. Through private communication with Professor Hamielec, he provided us the following dimensionless surface vorticity (ω_s) data for a circular cylinder and sphere.

Table III. Dimensionless surface vorticity, calculated by Hamielec

	Circular cylinder			Sphere	
	Re = 1	Re = 2	Re = 4	Re = 16	Re = 20
Angle	$-\omega_s$	$-\omega_s$	$-\omega_s$	$-\omega_s$	$-\omega_s$
0.0	0.0	0.0	0.0	0.0	0.0
6	0.1317	0.1845	0.2765	0.2173	0.7149
12	0.2607	0.3646	0.5455	0.4291	1.4017
18	0.3841	0.5359	0.7997	0.6337	2.0491
24	0.4996	0.6943	1.0327	0.8280	2.6404
30	0.6049	0.8365	1.2385	1.009	3.1606
36	0.6979	0.9593	1.4124	1.1746	3.5970
42	0.7772	1.0606	1.5509	1.3221	3.9396
48	0.8417	1.1386	1.6518	1.4498	4.1816
54	0.8905	1.1928	1.7141	1.5563	4.3201
60	0.9235	1.2229	1.7385	1.6407	4.3554
66	0.9409	1.2298	1.7266	1.7025	4.2921
72	0.9432	1.2149	1.6815	1.7417	4.1382
78	0.9314	1.1800	1.6070	1.7586	3.9049
84	0.9068	1.1278	1.5077	1.7541	3.6064
90	0.8709	1.0610	1.3889	1.7292	3.2587
96	0.8255	0.9826	1.2559	1.6854	2.8788
102	0.7723	0.8960	1.1143	1.6241	2.4839
108	0.7132	0.8042	0.9691	1.5472	2.0899
114	0.6500	0.7103	0.8253	1.4565	1.7111
120	0.5845	0.6171	0.6872	1.3539	1.3591
126	0.5180	0.5268	0.5584	1.2411	1.0424
132	0.4520	0.4416	0.4418	1.1199	0.7670
138	0.3874	0.3629	0.3395	0.9917	0.5359
144	0.3250	0.2915	0.2525	0.8584	0.3500
150	0.2651	0.2278	0.1810	0.7208	0.2082
156	0.2080	0.1717	0.1242	0.5800	0.1075
162	0.1534	0.1222	0.0805	0.4370	0.0434
168	0.1010	0.0782	0.0474	0.2924	0.00939
174	0.0501	0.0381	0.0218	0.1467	-0.00275
180	0.0	0.0	0.0	0.0	0.0

The dimensionless surface vorticity is related to the surface shear stress, β, as follows:

By definition

$$\beta = \left.\frac{\partial v_x}{\partial y}\right|_{y=0}, \qquad \text{(See Equation 43)} \tag{73}$$

and

$$\omega_s = -\left(\frac{\partial v_x}{\partial y} - \frac{\partial v_y}{\partial x}\right)\frac{R}{v_\infty} \tag{74}$$

At $y=0$, $v_y=0$, thus

$$\omega_s = -\frac{\partial v_x}{\partial y}\frac{R}{v_\infty}$$

$$= -\beta \frac{R}{v_\infty} \tag{75}$$

Figure 9 shows the dimensionless surface vorticity obtained by some of the authors mentioned previously. Sih's result at Reynolds number 5 was comparitively high because it was not calculated in an infinite medium. Southwell and Squire's result at Reynolds number 2 had a high maximum value as compared to Hamielec's result at Re = 2 and 4. Although the drag coefficient at Re = 2 by both Southwell and Squire and Hamielec seemed to agree (C_D = 1.519 and 1.527, respectively), the former was incorrect when compared to the limiting case Re $\to$ 0 [29]. At Re $\to$ 0, the stream function past a circular cylinder is

$$\psi = \left(\log \frac{3.703}{Re}\right)^{-1} \left(r \log r - \frac{1}{2} r + \frac{1}{2}\frac{1}{r}\right) \sin\theta \tag{76}$$

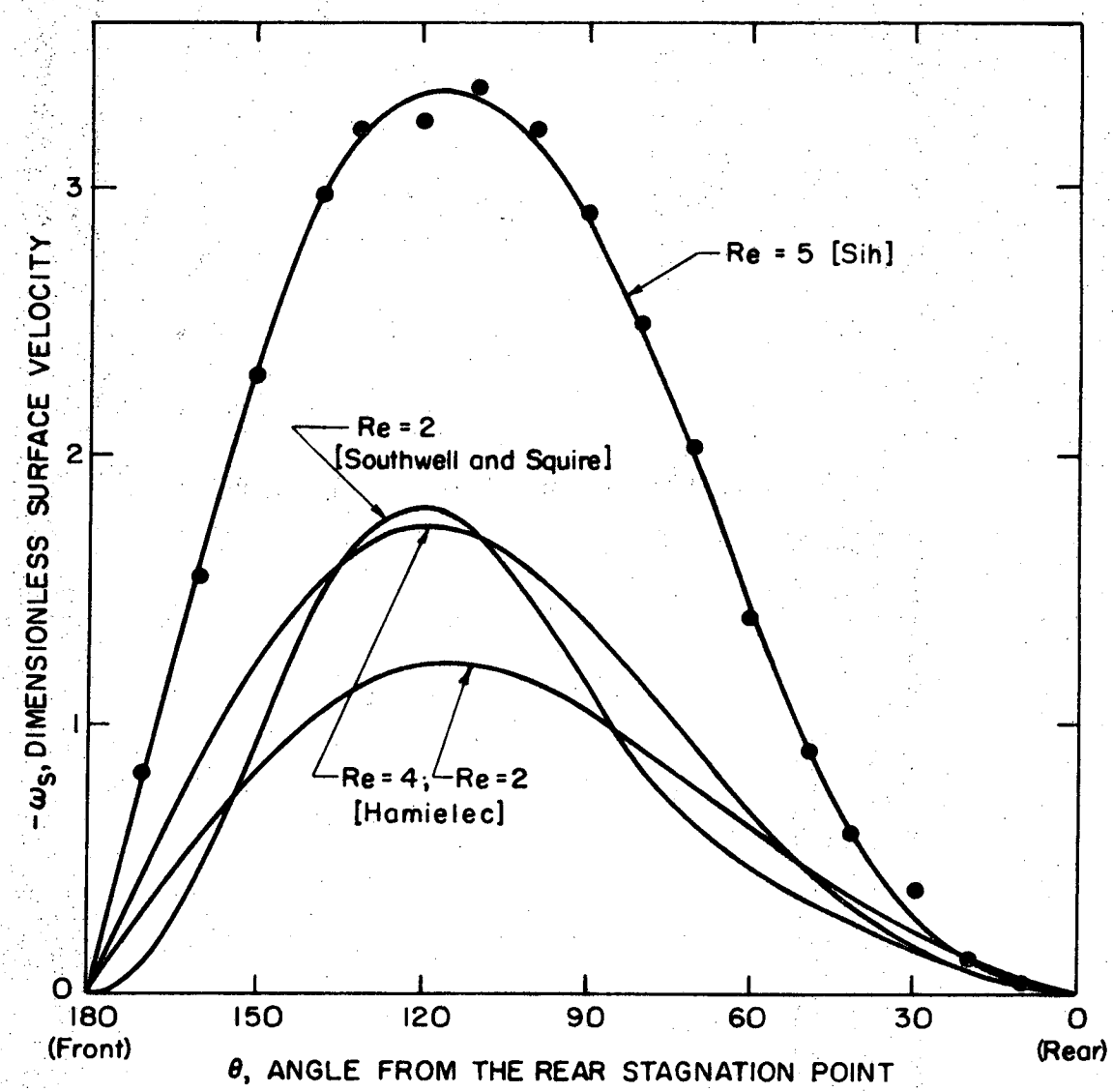

Fig. 9. Surface vorticity distribution for flow past a circular cylinder.

and for small $(\theta-\pi)$, the leading edge,

$$\omega_s \propto (\theta-\pi). \tag{77}$$

However, according to Southwell and Squire at Re = 2,

$$\omega_s = -\frac{\pi}{8}(4-\tau^2)(0.728 - 0.574\tau + 0.239\tau^2) \tag{78}$$

where $\tau = 2\cos(\theta-\pi)$ (79)

for small $(\theta-\pi)$

$$\omega_s \propto (\theta-\pi)^2 . \tag{80}$$

Clearly, it contradicted the limiting case. Consequently, we consider Hamielec's results as being more nearly correct.

The composite solution for the mass flux to a circular cylinder can be expressed as:

$$\underline{N} = \underline{N}_{bl} + \underline{N}_r - \underline{N}_r \quad (X \to \infty) \tag{81}$$

where the subscripts bl and r denote the diffusion boundary layer and the rear region respectively. By rearranging Equation (55), (56), (62) and (63) one can obtain

$$\underline{N} = -\frac{D(C_\infty - C_o)}{\Gamma(4/3)} \left\{ \frac{\sqrt{\beta}}{\left[9D \int_o^x \sqrt{\beta}\, dx\right]^{1/3}} + (A/D)^{1/3} \left[\frac{\sqrt{D}}{9\int_o^{x_o} \sqrt{\beta}\, dx}\right]^{1/3} \left[\left.\frac{\partial\overline{\Theta}}{\partial Y}\right|_{Y=0} - \sqrt{X}\right] \right\} . \tag{82}$$

Using the diameter of the circular cylinder as the characteristic length, one can express the mass flux in terms of the local Nusselt number

$$Nu = -\frac{\underline{\underline{N}} \cdot 2R}{D(C_\infty - C_o)}$$

$$= \frac{2R}{\Gamma(4/3)} \left\{ \frac{\sqrt{\beta}}{\left[9D \int_o^x \sqrt{\beta}\, dx\right]^{1/3}} \right.$$

$$\left. + (A/D)^{1/3} \left[\frac{\sqrt{D}}{9 \int_o^x \sqrt{\beta}\, dx}\right]^{1/3} \left[\left.\frac{\partial \bar{\Theta}}{\partial Y}\right|_{Y=0} - \sqrt{X}\right] \right\} . \qquad (83)$$

Similarly, the Nusselt number for a sphere

a) in Stokes flow is

$$Nu = \frac{2}{(Pe/2)^{-1/3}} \cdot \frac{\sin\theta}{\Gamma(4/3)\, 3^{1/3} \left[\pi - \theta + \frac{1}{2} \sin 2\theta\right]^{1/3}}$$

$$+ Nu_r(S) - \frac{2S}{\Gamma(4/3)(3\pi)^{1/3}} . \qquad (84)$$

($Nu_r(S)$ is plotted in Figure 5.)

b) in low Reynolds number flows is

$$Nu = \frac{2R}{\Gamma(4/3)} \left\{ \frac{\sqrt{P\beta}}{\left[9D \int_o^x P\sqrt{P\beta}\, dx\right]^{1/3}} \right.$$

$$\left. + \frac{(2A/3)^{1/3}}{\left[4\sqrt{A} \int_o^x P\sqrt{P\beta}\, dx\right]^{1/3}} \left[\left.\frac{\partial \bar{\Theta}}{\partial Y}\right|_{Y=0} - S\right] \right\} . \qquad (85)$$

($P = R \sin\theta$ for a sphere.)

Figures 10 and 11 show some of the results calculated according to Equations (83), (84), and (85). The physical system chosen for the calculations was potassium ferricyanide, potassium ferrocyanide, both at a concentration of 1.5×10^{-2} moles/liter, and sodium hydroxide at 1 N. The diffusion coefficient at 25°c is 8.809×10^{-6} cm^2/sec. The experimental results from a benzoic acid sphere were obtained by Garner and Keey [5].

It was especially interesting to note in Figure 10 that the mass transfer rates based on the Southwell and Squire's shear stress distribution was totally erroneous. It predicted zero mass flux at the front stagnation point, since $d\beta/d\theta \rightarrow 0$ at that point. Also, it appeared that the mass flux at the rear stagnation point decreased with increase in Reynolds number. This is reasonable since at high flow rates, mass transfer in the front region increases; consequently, the solution becomes more depleted at the rear region.

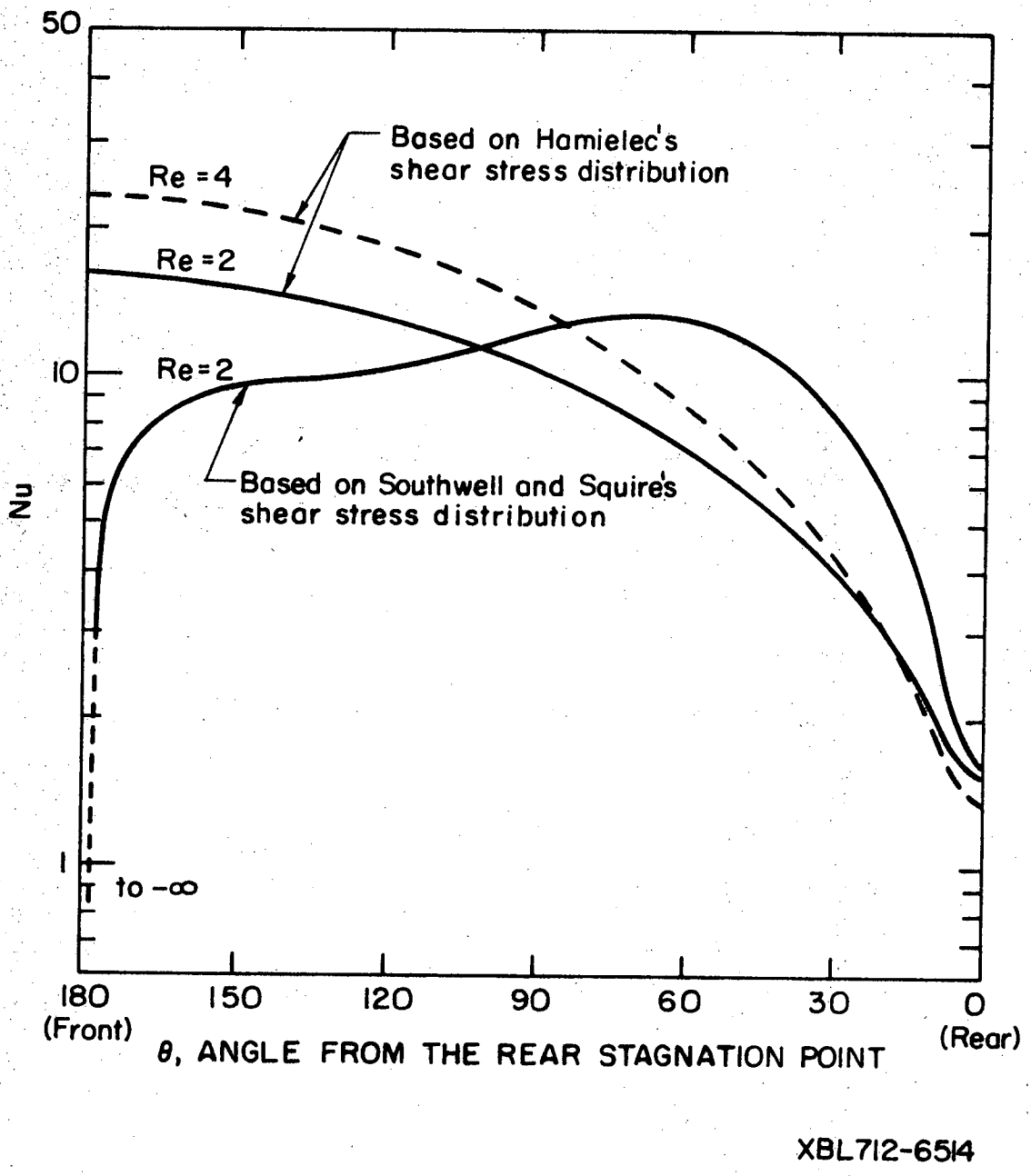

Fig. 10. Mass transfer to a circular cylinder.

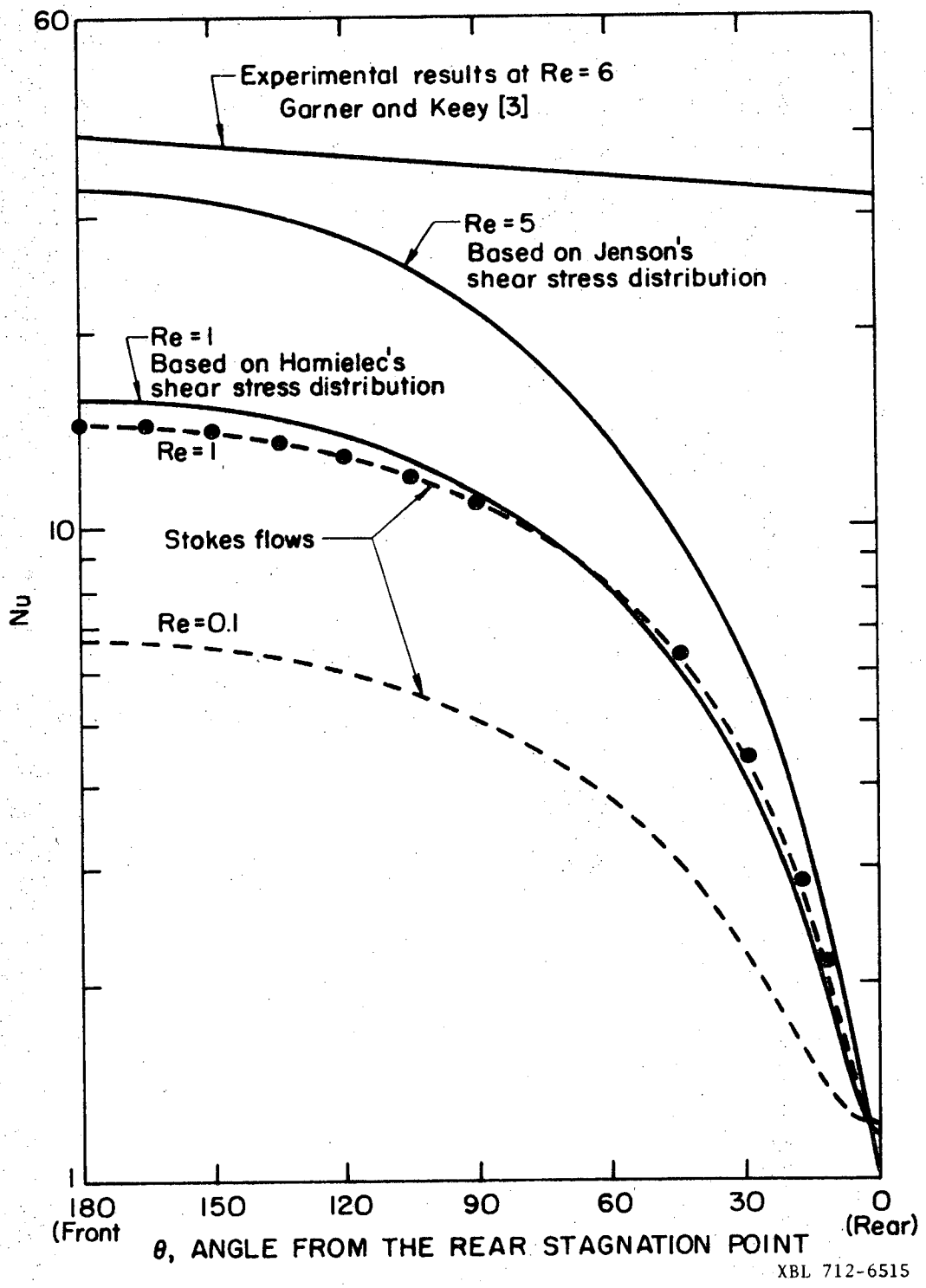

Fig. 11. Mass transfer to a sphere.

CHAPTER IV. SHEAR STRESS MEASUREMENT BY A SHORT ELECTRODE

In the preceding chapter an illustration was made for the computation of the local mass transfer rates to a circular cylinder in terms of the shear stress distribution. However, these shear stress distributions were based on a circular cylinder in an infinite medium. The flow tunnel (See Chapter V, section A) used in the experiment had a square cross-sectional area of 36 inch^2 (or 6 inches x 6 inches), and the circular cylinder had a diameter of 1/4 inch. Such a combination definitely does not adhere to the infinite medium condition. Consequently, one must determine the shear stress distribution for this particular system experimentally. This can easily be achieved. The diffusion layer solution, Equations (55) and (56), indicates that if only a small section of the cylinder is undergoing mass transfer (i.e., x is small), β may be considered as being constant. Hence, by measuring the mass flux to such a section the local shear stress can be obtained. Dimopoulos' [6] work on the shear stress distribution as well as other work by Hanratty [10], [11], [12] were entirely based on this idea. Figure 12a shows a cylinder constructed for this purpose. A small electrode was embedded in a lucite cylinder. Current to the electrode can then be used to calculate the local shear stress. Incidentally, this cylinder is nearly a replica of what Dimopoulos used, except its dimensions are smaller.

It may be of interest to note that the electrode for shear stress measurement must be embedded in an insulating cylinder. One cannot use the two-electrode cylinder discussed in the introduction (See Figure 3, page 8), for even though no net current is passed to the large electrode,

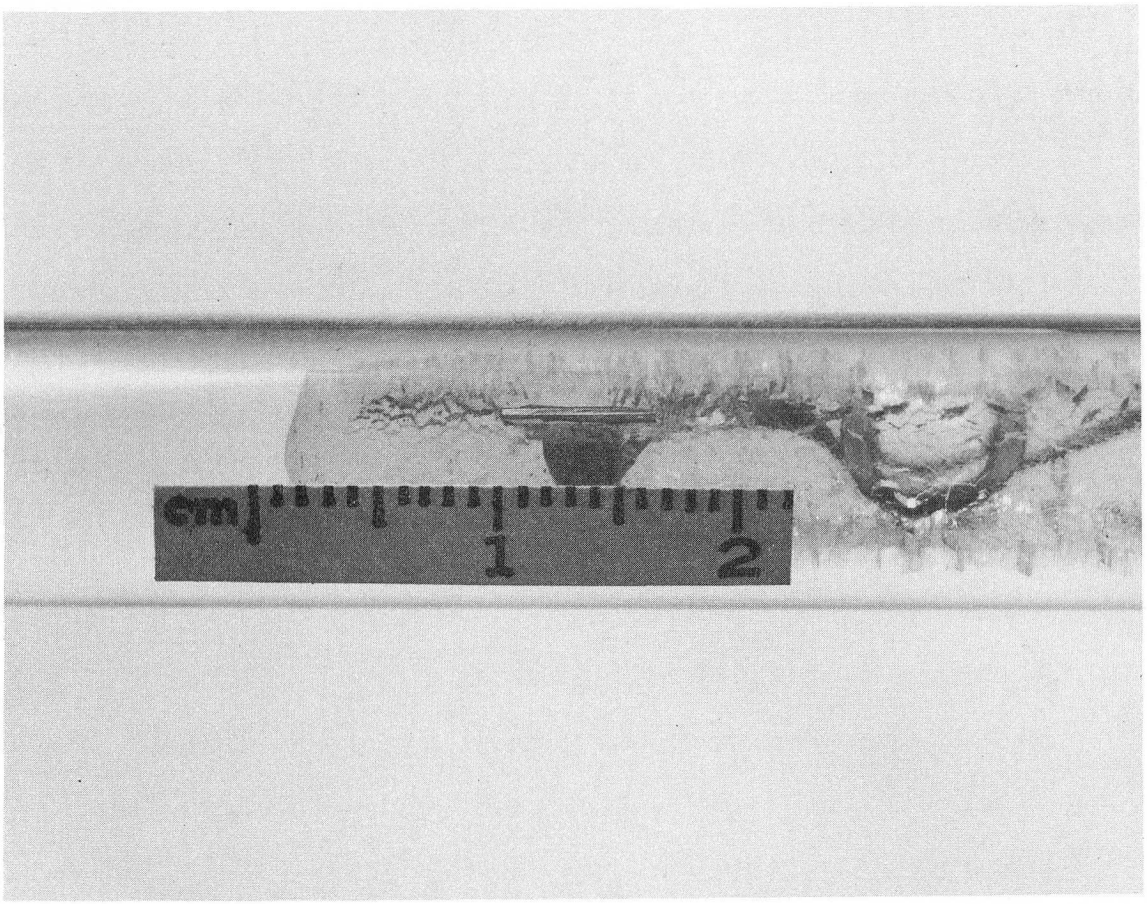

XBB714-1780

Fig. 12a. Circular cylinder with one electrode for shear stress distribution measurements.

there can be local reactions at the large electrode which enhance the current to the small electrode. Figure 12b illustrates such a situation.

Since the dimension of the electrode is very small, we felt that edge effects could be important. The diffusion layer solution did not take this into account. Newman [30] recently studied a variety of problems by the same theoretical approach as shown in Chapter I and II. One of these involved the mass transfer rates at the leading and trailing edges of a flat plate which could be applied to the problem at hand. Below is a brief summary of the development of equations and results. The mathematical details and various practical implications are currently being written into a paper for publication.

Let us consider a small lengthwise strip of the circular cylinder. When it is sufficiently small, it may be considered as a flat plate. The diffusion equation of this small electrode in terms of the dimensionless concentration is

$$v_x \frac{\partial \theta}{\partial x} + v_y \frac{\partial \theta}{\partial y} = D\left(\frac{\partial^2 \theta}{\partial x^2} + \frac{\partial^2 \theta}{\partial y^2}\right) \tag{75}$$

where x is along the surface and y is normal to the surface. For uniform shear rate the velocity profile is given by

$$v_x = \beta_o y, \quad v_y = 0 \tag{76}$$

where β_o = the shear rate.

As we stated in Chapter II we are only interested in the case of large Peclet number, defined for this small electrode as

$$Pe = L^2 \beta_o / 2D. \tag{77}$$

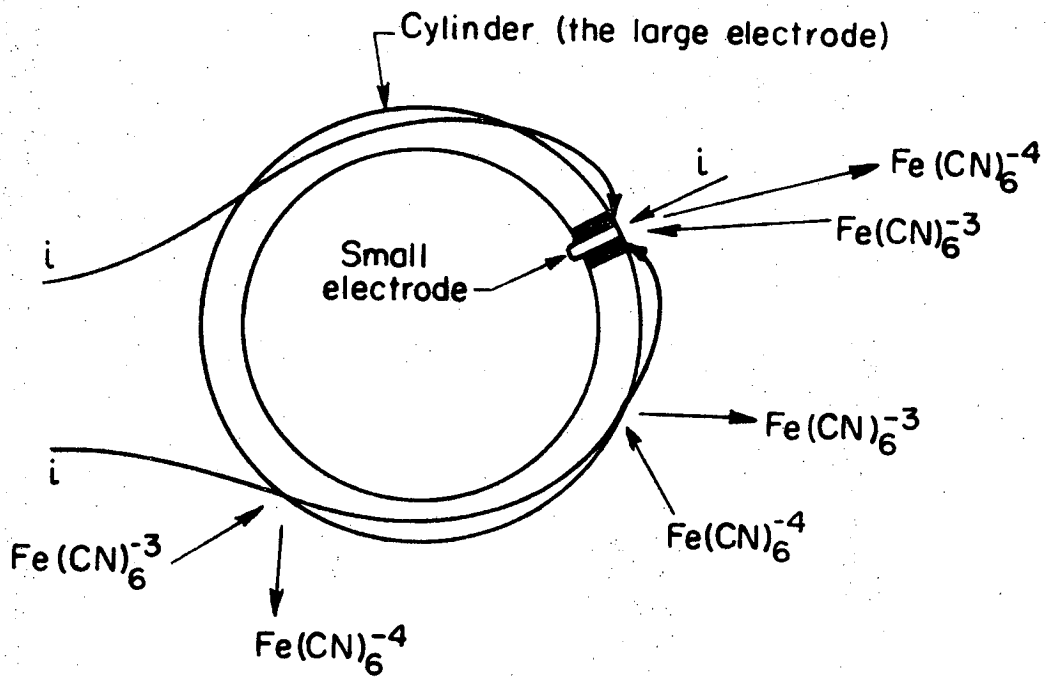

Fig. 12b. Current through the large electrode (net current is zero) when only the small electrode is connected to a current source.

where L is the length of the plate. In this case, the mass-transfer mechanism can be divided into four regions -- regions A, B, C, D (See Figure 13). Region C is the leading edge of the mass-transfer surface with the appropriate variables being

$$X_C = x\sqrt{\beta_o/2D} \ , \quad Y_C = y\sqrt{\beta_o/2D} \ . \tag{78}$$

Equation (75) becomes

$$2Y_C \frac{\partial\Theta}{\partial X_C} = \frac{\partial^2\Theta}{\partial X_C^2} + \frac{\partial^2\Theta}{\partial Y_C^2} \tag{79}$$

with boundary conditions

1. $\Theta = 0$ at $Y_C = 0$, $X_C > 0$.
2. $\partial\Theta/\partial Y_C = 0$ at $Y_C = 0$, $X_C > 0$.
3. $\Theta \to 1$ as $X_C \to -\infty$ or as $Y_C \to \infty$.
4. as $X_C \to \infty$, $\partial^2\Theta/\partial X_C^2 = 0$.

The numerical solution was presented in Reference 31. The concentration gradient at the surface of the leading edge is reproduced here as Figure 14.

Boundary condition 4 arises from the fact that one expects the concentration gradient along x to diminish when $X_C \to \infty$. Equation (79) then becomes

$$2Y_C \frac{\partial\Theta}{\partial X_C} = \frac{\partial^2\Theta}{\partial Y_C^2} \ . \tag{80}$$

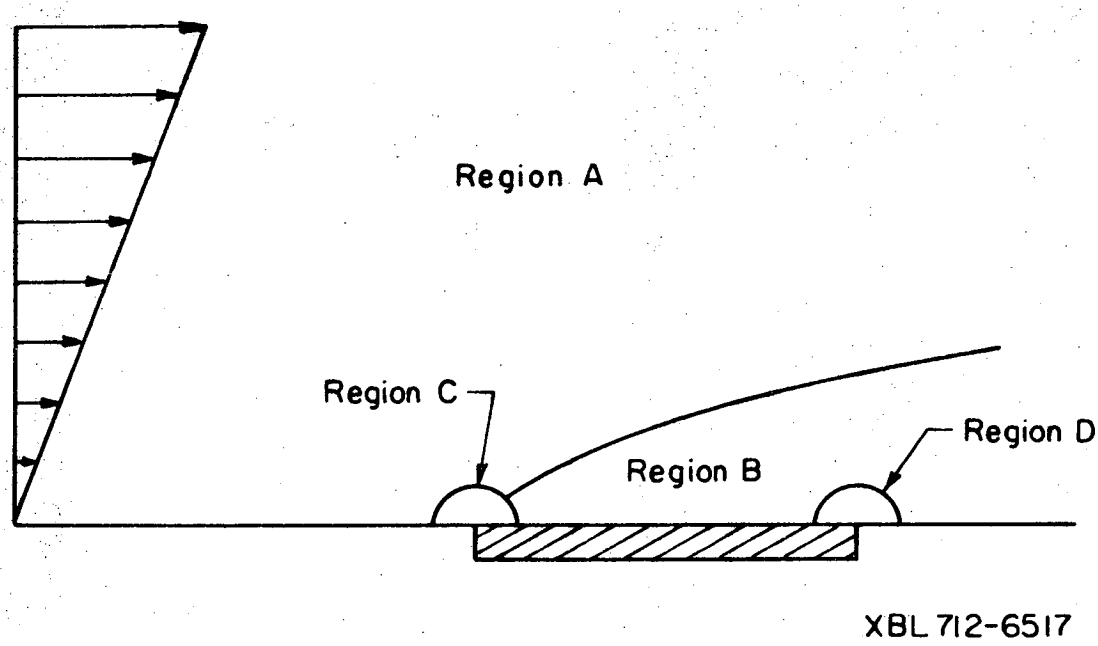

Fig. 13. Mass transfer to a flat plate in uniform shear.

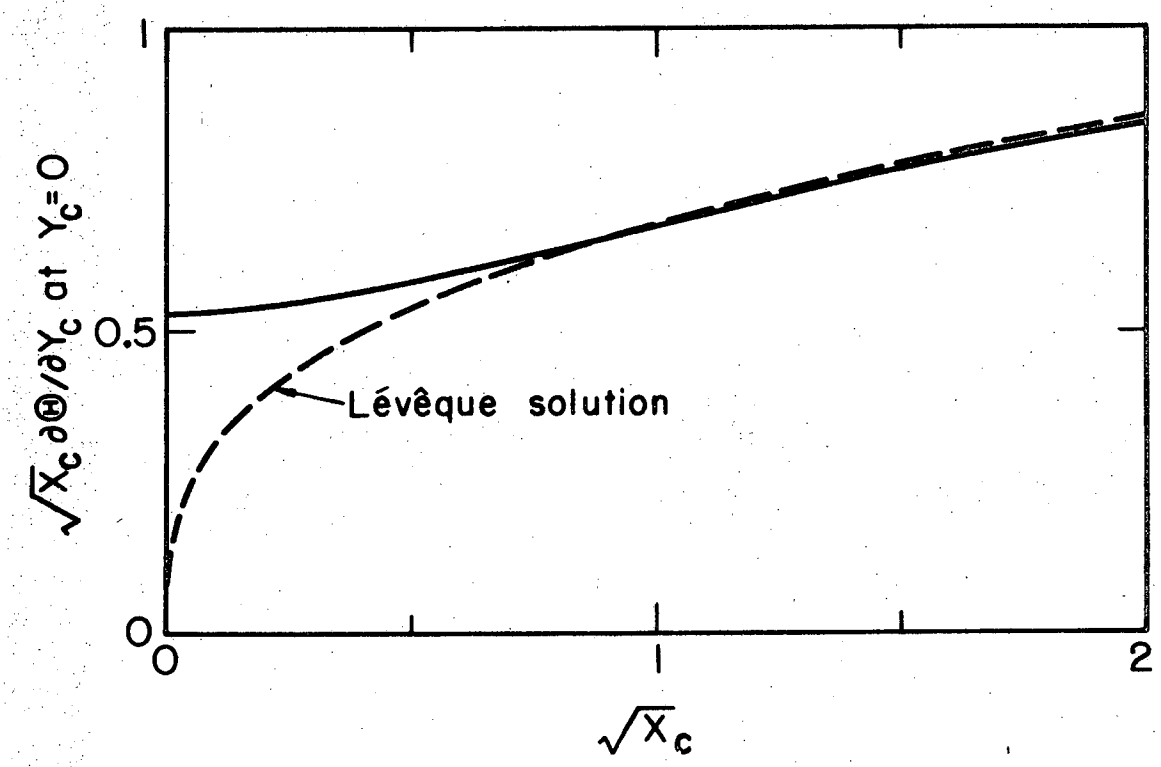

Fig. 14. The normal concentration derivative at the wall in the elliptic region at the beginning of the mass-transfer section, with the Lévêque solution for comparison.

This equation has a similarity solution of the form

$$\Theta \rightarrow \frac{1}{\Gamma(4/3)} \int_0^{\eta} e^{-x^3}\, dx \tag{81}$$

where

$$\eta = Y_C(2/9X_C)^{1/3} \quad . \tag{82}$$

This is the familiar Lévêque [13] solution, and as one will see, it is also the solution for region B.

For region B the appropriate variables are

$$X_B = x/L \quad \text{and} \quad Y_B = y(\beta_o/LD)^{1/3}. \tag{83}$$

Substitution into Equation (75) yields

$$Y_B \frac{\partial \Theta}{\partial X_B} = \frac{\partial^2 \Theta}{\partial Y_B^2} + (2Pe)^{-2/3} \frac{\partial^2 \Theta}{\partial X_B^2} \tag{84}$$

It is obvious, as $Pe \rightarrow \infty$, diffusion in x-direction becomes negligible and Equation (84) reduces to

$$Y_B \frac{\partial \Theta}{\partial X_B} = \frac{\partial^2 \Theta}{\partial Y_B^2} \tag{85}$$

with boundary conditions:

1. $\Theta = 0$ at $Y_B = 0$.

2. $\Theta \rightarrow 1$ as $Y_B \rightarrow \infty$.

3. As $X_B \to 0$, solution in region B must match the solution in region C as $X_C \to \infty$.

Equation (85) is parabolic. An important consequence is that there will not be any upstream propagation of effects from the trailing edge, region D.

The solution presented by Equation (81) satisfies all the boundary conditions for Equation (85) except η has the form of $Y_B(1/9X_B)^{1/3}$. Accordingly, it is proper to say that the diffusion layer, region B, is merely an asymptotic part of region C. Region D at the trailing edge of the mass-transfer section has

$$X_D = (x - L)\sqrt{\beta_o/2D},$$

$$Y_D = y\sqrt{\beta_o/2D},$$

$$\overline{\Theta} = \Theta\, Pe^{1/6}\Gamma(4/3)(9/2)^{1/3} \tag{86}$$

as its appropriate variables. Its differential equation is

$$2Y_D \frac{\partial\overline{\Theta}}{\partial x_D} = \frac{\partial^2\overline{\Theta}}{\partial x_D^2} + \frac{\partial^2\overline{\Theta}}{\partial Y_D^2} \tag{87}$$

with boundary conditions

1. $\overline{\Theta}_D = 0$ at $Y_D = 0$, $x_D < 0$.

2. $\partial\overline{\Theta}/\partial Y_D = 0$ at $Y_D = 0$, $X_D > 0$.

3. $\overline{\Theta} \to Y_D$ as $Y_D \to \infty$,

4. as $X_D \to \infty$, $\partial^2\overline{\Theta}/\partial X_D^2 \to 0$.

The last boundary condition again arises from the anticipation of a diminishing concentration gradient along the x-direction. An asymptotic solution of Equation (87) with this boundary condition can be found. However, it will not be dealt with here. The solution for region D is presented in reference 32. The normal concentration gradient along the trailing edge is shown in Figure 15.

The total mass transfer rate can be obtained by forming the composite solution of regions B, C, and D.

In terms of the Nusselt number, it is

$$Nu = \int_0^L \left.\frac{\partial \Theta}{\partial y}\right|_{y=0} dx$$

$$= 1.0175\ Pe^{1/3} + \frac{0.3 + 0.3288}{Pe^{1/6}} + O(Pe^{-1/3}) \qquad (88)$$

Equation (88) is a "working" equation since the Nusselt number can be measured experimentally.

$$Nu = \frac{QL}{D(C_\infty - C_o)} \qquad (89)$$

where Q = mass flux, moles/sec-cm^2

L = characteristic length of the flat plate

D = diffusivity

C_∞ = bulk concentration

C_o = surface concentration.

The corresponding Peclet number can be calculated by solving the third order equation in terms of $Pe^{1/6}$.

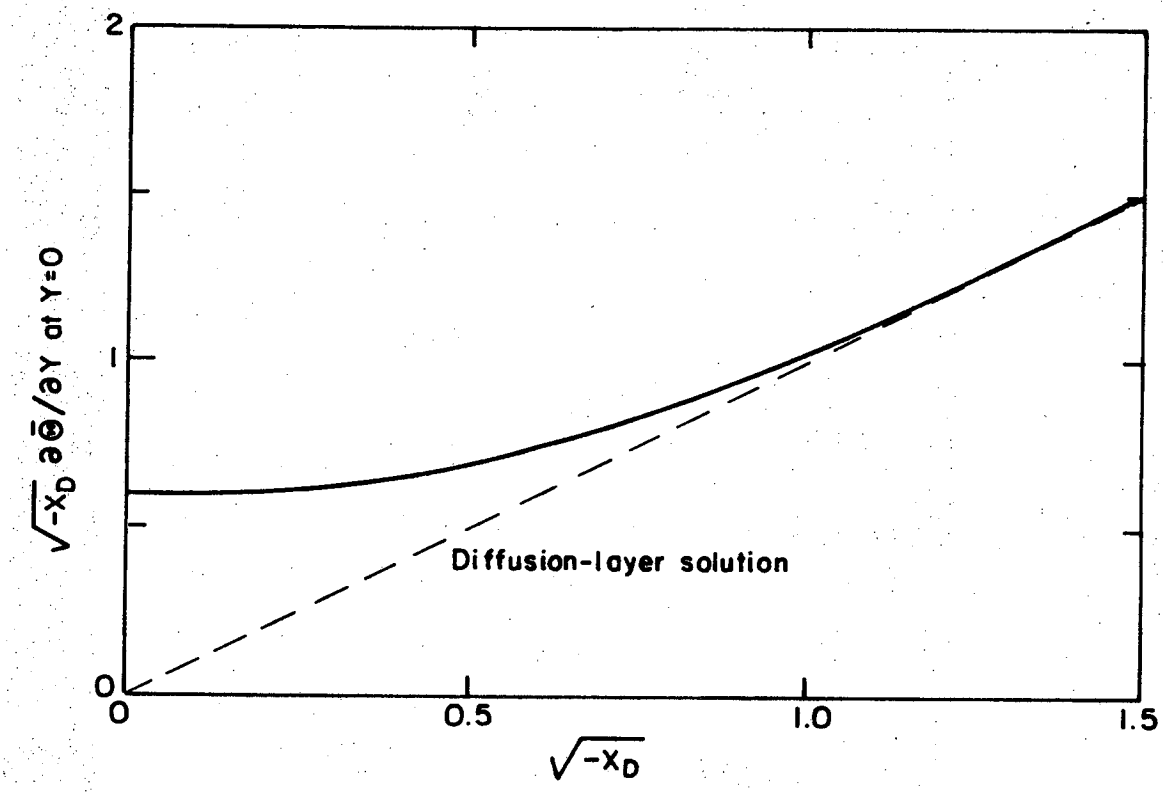

Fig. 15. Mass-transfer rate near the trailing edge of a flat plate under uniform shear rate.

It may be interesting to point out here that without the leading and trailing edge corrections Equation (88) corresponds to the equation used by Dimopoulos [6]; that is,

$$Nu = 0.807\ Z^{1/3} \ . \tag{90}$$

The constant is different, however, because Dimopoulos defined Z as $(2\ Pe)^{1/3}$.

CHAPTER V. EXPERIMENTAL MEASUREMENT OF MASS TRANSFER RATES TO A CIRCULAR CYLINDER IN LOW REYNOLDS NUMBER FLOW

As mentioned in the Introduction, the electrochemical system, potassium ferricyanide, potassium ferrocyanide, in excess supporting electrotyle, KNO_3 - seemed to be ideal for our purpose. And the object which seemed particularly suitable for the experiment and theoretical treatment was a circular cylinder. What were lacking seemed to be a suitable flow system and a temperature control system. In this chapter we shall deal in detail with the construction of these systems as well as the very involved and delicate assemblage of the 2-electrode circular cylinder. In addition, the overall experimental setup and experimental procedures will be discussed.

A. The Flow System

The flow tunnel, originally designed by Tom Atkins [21] but never assembled nor tested, was modified extensively for this experiment. The prototype moving-wall section was removed due to excessive vibration from the movement of the gears as well as the moving walls. A straight, square cross-sectional area tunnel was installed. Figure 16 shows the entire flow system with the flow tunnel. The total straight section was 34" long. It was made of lucite 1/4" thick. Seven portholes, with sealing plugs, of 1" in diameter were made on each side of the walls. The two used in this experiment were 17" from the start of the straight section. The inlet and outlet sections were made of stainless steel, and each was 23" long. The inlet section had an elbow while the outlet section had a tee. In the inlet section two stainless steel screens were glued in place by epoxy. The purpose was to create a more uniform

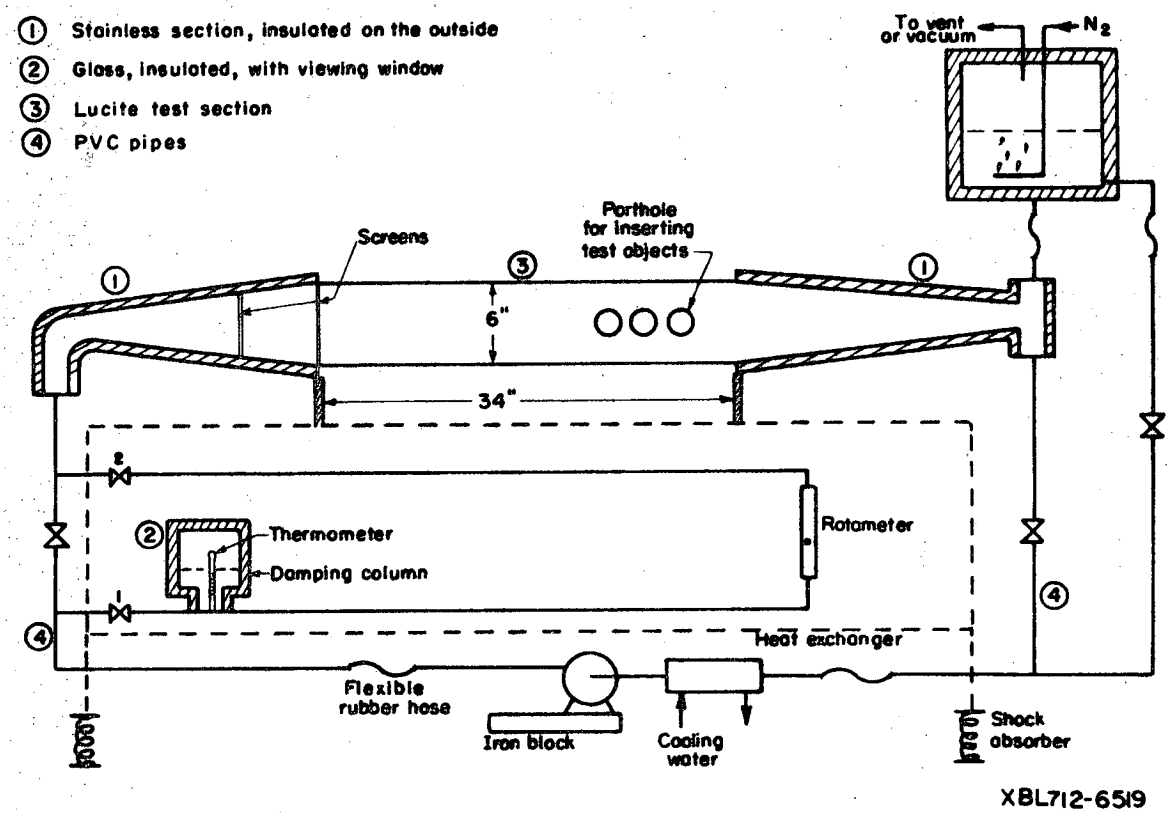

Fig. 16. Flow system.

flow. Since both sections were made of metal, heat transfer with the surroundings was too fast. Therefore, both sections were insulated with asbestos material. The piping arrangement of the flow system was very simple. PVC pipes were used exclusively, because they were corrosion resistant and poor in heat transfer. Preceding the inlet to the flow tunnel, a damping section was added to absorb the high frequency oscillation caused by the centrifugal pump. This section consisted of a damping column, a section of 80" long 1" pipe, a rotameter and two restriction valves. In principle, by restricting the flow at valve two the oscillation energy in the flow could be absorbed and released by the gas (N_2) in the column. The design of this section is discussed in Appendix C. The steady position of the glass float in the rotameter indicated that a steady flow was maintained. To avoid heat exchange at the damping column (glass), it was also insulated except for a window, through which the thermometer in the column could be observed.

The constant-head reservoir provided steady pressure to the pump and the entire system. It contained a stainless tube with fine holes for purging the solution with nitrogen and a vent which could be connected to a vacuum. It had two purposes, one of them was to help degas the solution. The other will be mentioned in the procedure section.

Prior to the pump a small heat exchanger was installed to maintain the fluid at constant temperature. It consisted of a piece of stainless pipe jacketed concentrically by a copper cover. Cooling water was circulated between them.

The centrifugal pump was stainless steel, made by R. S. Corcoran Co. (Model 2000 F). It was driven by a variable speed motor made by Bodine,

1/2 hp, the motor controller was manufactured by Minarik (variable speed system, Model SH-73).

The flow system was literally suspended by springs and soft rubber pads. First, a stand was constructed to support the flow tunnel. Attached to each of its legs was a shock absorbing spring. These springs were purchased after determining the average weight on the legs. They were designed to absorb building vibrations. Furthermore, the flow tunnel was held up on the stand by laboratory jacks. The top and bottom of these jacks were padded with soft rubber pads. The constant-head reservoir was held up by a platform connected to the ceiling. It was also isolated away from the building by rubber pads. The motor and pump were bolted on an iron block. The added weight reduced the amplitude of the vibration by these machines. The block's bottom side was again padded to reduce its impact to the floor. In addition to these precautions, rubber hoses were used near the pump and the constant-head reservoir so that vibration from the equipment could not propergate through the rigid pipes. See Figure 16 for details.

B. Temperature Control System

The entire laboratory room was air-conditioned at a temperature about 22°C. The entire apparatus was placed inside a walk-in hood--about 8 feet high, 5 feet wide, and 15 feet long. The walls and doors of this hood were insulated with a 1" thick fiber glass sheet. The inside of the hood was maintained at 24°C by small light bulbs controlled with a temperature relay system. The accuracy was within 0.01°C. To insure uniform temperature within the hood two fans were installed to circulate the air inside. The motor which drives the centrifugal pump was placed

in a fiber glass insulated box. The air supply to this box was passed through a tapwater tank whose water had just passed through a constant temperature bath to keep the air at a relatively constant termperature. This air was then led into the insulated box. A vacuum at the opposite end of the box takes away the warmed air. In this manner a relatively constant temperature was maintained around the motor and the heat conduction to the pump was also kept at a relatively constant rate. To control the temperature of the fluid, it was cooled prior to the entrance into the pump via a heat exchanger. The cold water to the heat exchanger was supplied from a constant temperature reservoir whose temperature was maintained at about 18°C with an accuracy of 0.01°C. The flow rate of the cooling water was adjustable so that the fluid of the system was maintained at 24°C with fluctuations no more than 0.05°C. To observe the temperature of the system, a thermometer was placed inside the damping column which was in direct contact with the fluid coming out of the pump. A thermometer was also installed in the flow tunnel to indicate the temperature there. In addition, the entire flow tunnel was surrounded by fiber-glass insulations acting as buffers. This arrangement reduced the chances of the tunnel coming in contact with any high or low temperature gases. A schematic diagram of the temperature control system is shown in Figure 17.

C. Electrode Construction

The concept of the 2-electrode object was mentioned in the introduction, and a simple sketch was shown in Figure 3. However, the actual construction of such a system proved to be extremely difficult and required immense patience and delicate workmanship. Figure 18 shows the

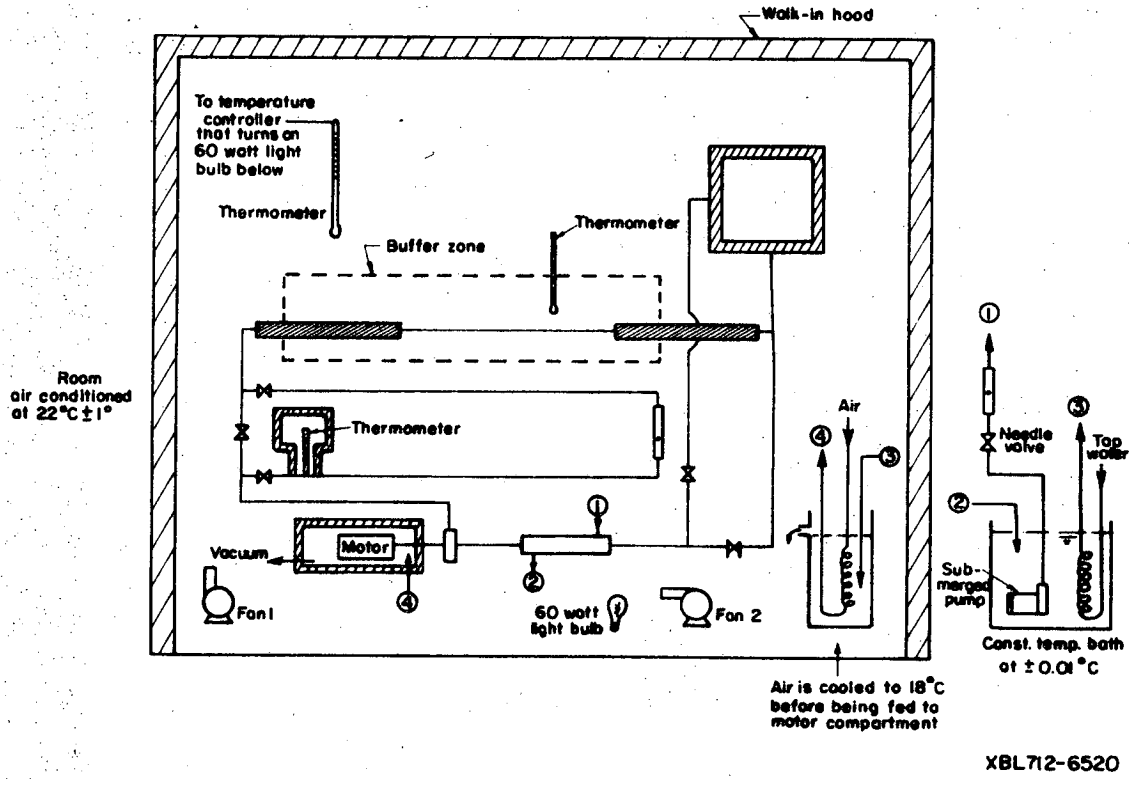

Fig. 17. Temperature control system.

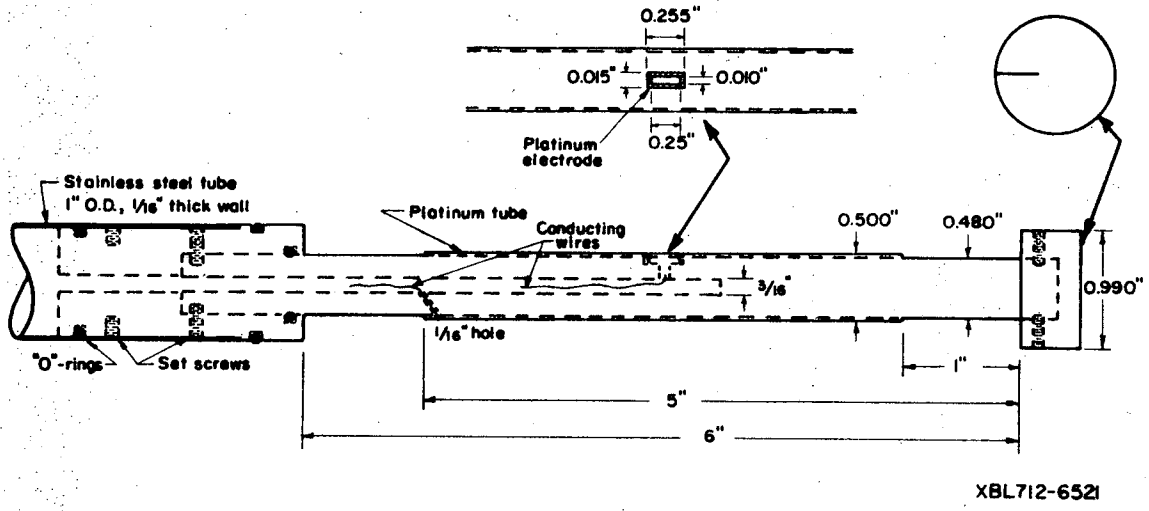

Fig. 18. Structure of mass transfer circular cylinder - a 2-electrode object.

structure in detail. Figure 19 is a picture of the actual cylinder.

Basically, the cylinder was composed of a lucite rod, 6 inches long and 0.480 inches in diameter, whose central portion was covered by a platinum tube, 4 inches long and 0.500 inches in the outer diameter. A small piece of the platinum 0.015 " x 0.255 " was removed from the tube, through which another platinum electrode was inserted. The gap between the two platinum pieces is less than 0.003 " as one can see from Figure 18. When properly isolated with Epoxy glue, they formed a 2-electrode system. One of the difficulties encountered during construction was that the Epoxy tended to form bubbles during curing; consequently, it left an uneven surface as well as leakage of solution into the electrical lead wires causing corrosion. The problem was resolved by degassing the Epoxy before applying, and during curing a slight vacuum was applied at the "electrical-wire" side. In this manner a slight pressure gradient was created to allow the excess gas to escape through the vacuum as well as to assure complete filling of the gaps between the electrodes. Although at this stage it is immaterial to recount the many unsuccussful models, it is sufficient to say that this final, workable version evolved not from accident, but from many heartbreaking failures. In Appendix B, a brief description about the construction of the platinum tube was presented. Incidently, Dimopoulos used a round platinum wire as the small electrode for his mass transfer study. The area occupied by the epoxy was not specified, although from the sketches presented, it seemed much larger than the wire itself. For the slow flow rates involved here, we considered it inadequate.

To measure the shear stress distribution, a lucite cylinder, 0.500 " O.D., with just one small electrode embedded in it was also constructed. As might be expected, it was much easier to make.

To facilitate the insertion and extraction of the object, a "side-arm" was placed at the object porthole on the tunnel. A drawing of it is shown in Figure 20. It consisted of an 1-1/2" lucite tube with a Lawrence Radiation Laboratory Wilson seal on one end and a 1-1/2 " ball valve in the middle. To remove the object, it was first pulled between the Lawrence Radiation Laboratory Wilson seal and the ball valve and then the valve was closed. The solution trapped between the two was drained out but saved. The Lawrence Radiation Laboratory Wilson seal and the object could then be removed simultaneously. To insert the object the reverse procedure was used.

D. Electrical Circuit

The electrical circuit of the system is shown in Figure 21. The two major pieces of equipment used were 1) a potentiostat, the current or voltage source, and 2) an operational amplifier. The potentiostat was manufactured by G. Bank Elektronik of Germany. The operational amplifier was a chopper stablized operational amplifier, model 231 J by Analog Devices. Power supply to the amplifier was a model 901 D.C. power supply, also, by Analog Devices.

Following Figure 21 and starting from the cathodes: the circular cylinder, the larger electrode, was connected to the negative terminal of the potentiostat while the small electrode passed through the amplifier to the same negative terminal. The positive terminal was connected to the downstream, outlet section of the flow tunnel, made of stainless steel,

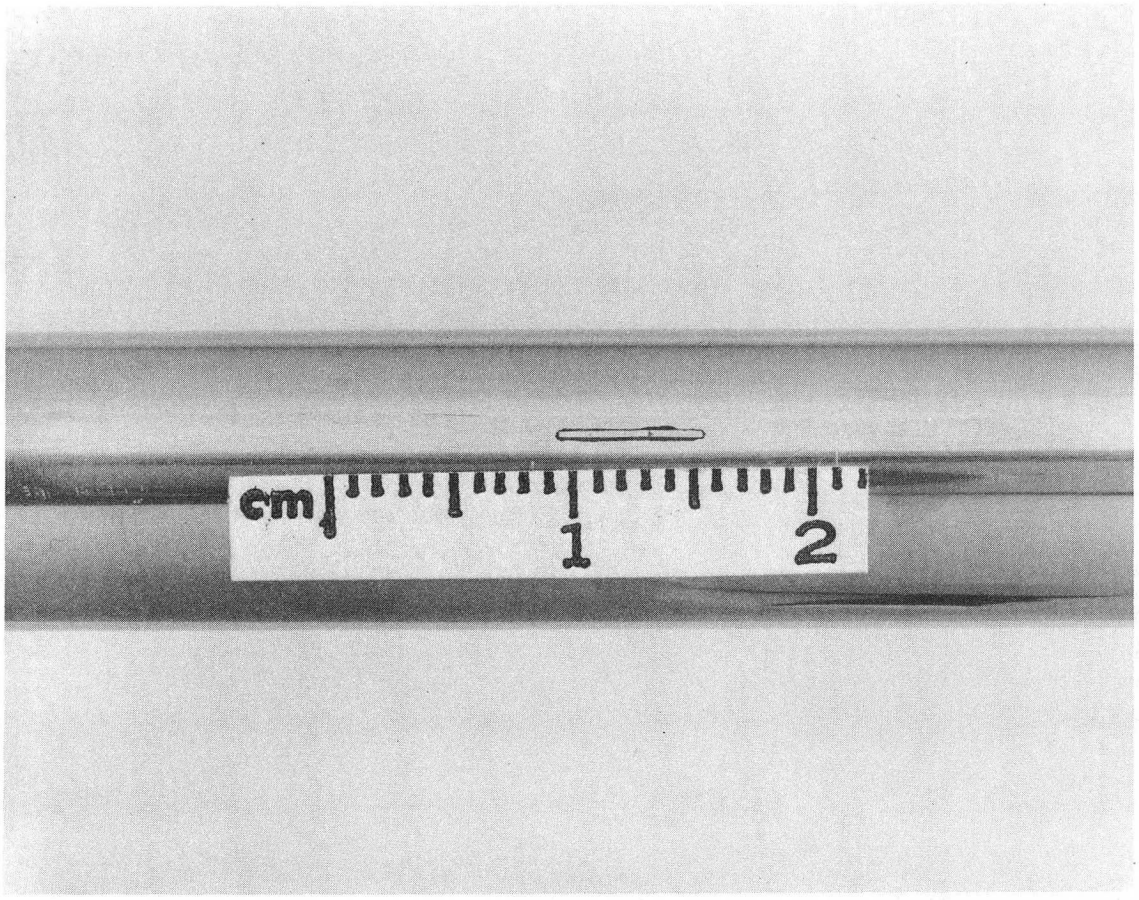

XBB714-1781

Fig. 19. Circular cylinder with 2-electrodes for mass transfer rate measurements.

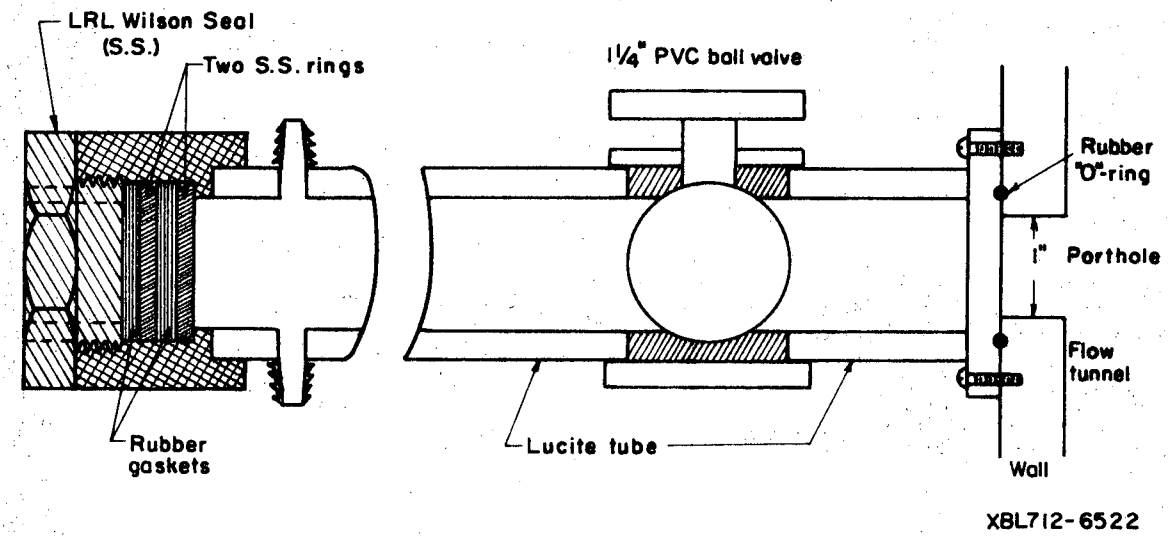

Fig. 20. Side-arm on the flow tunnel for inserting the test objects.

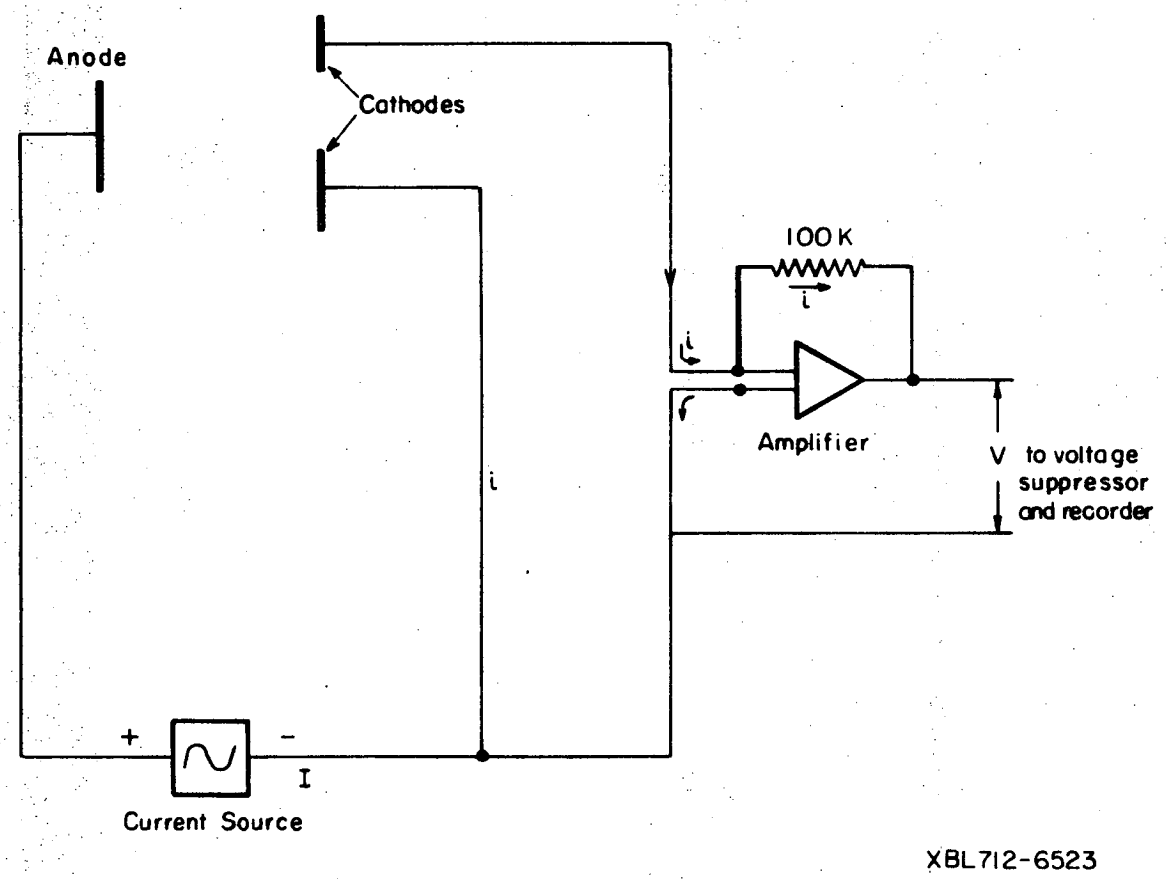

Fig. 21. Electrical circuit.

as the anode. The reference terminal of the potentiostat was shorted to the positive terminal. Initially, a platinum reference electrode was connected to the reference terminal and the electrode was placed at various parts of the system. It did not show any difference in the current-potential relationship. Hence, we simply connected the reference and the positive terminals together. The platinum electrode was also used as the anode to check the effect of the stainless steel anode. No difference in current potential relationship could be observed either. Also, note, the potentiostat was internally grounded through the cathode. Consequently, it was necessary to electrically float the system by an isolation transformer and to make all the stainless steel parts of the system part of the anode.

The operational amplifier had a 100K resistor. The current passing through the resistor corresponded exactly to that of the small electrode. The leakage current in this device was 10^{-12} or less amperes. This was very small compared to 10^{-6} amperes, the current through the small electrode. The output voltage was then sent to a suppressor to compensate for a large portion of the output. Normally, a voltage of less than 100 mV was sent to a t,Y-recorder. In this manner, small changes in the voltage output could be observed. The recorder was made by Sargent, model SRG.

To impose a potential between the anodes and cathodes, one simply set the desired potential at the potentiostat.

E. Velocity Profile Determination

Various attempts were made to measure the velocity profile in the flow tunnel, but we failed to find a suitable means to do the job. The difficulty arose from the fact that for a cylinder of 0.500 inches, and $\rho = 1.0151\ g/cm^3$, $\mu = 0.8909$ cp (see physical properties section), the flow rate at Reynolds number 5 was only 0.04 cm/sec. Under this extreme condition dyes tended to disperse after only traveling a short distance. A hot-wire anemometer generated too much natural convection, and the signals were too low for measurement.

However, according to Han [33], the entrance length of a square tunnel is

$$L_e = 0.0752\ D_e\ Re_t \tag{90}$$

where

D_e = the tunnel's hydraulic diameter.

Re_t = tunnel Reynolds number.

One of the tunnel Reynolds number used in the experiment was 36.88 which yielded from Equation (90) Le = 16.6 inches. The object porthole was 17 inches from the beginning of the straight section; therefore, we should expect a fully developed velocity profile at that position. Han also stated that when fully developed

$$\frac{u_o}{u_\infty} = 2.0977 \tag{91}$$

where u_o = central line velocity.

u_∞ = average velocity.

Correspondingly, the object was confronted with a flow which yielded a Reynolds number of 6. Since the velocity profile was nearly parabolic, the overall Reynolds number could be less than 5.

We did not pursue this matter further as we felt that the more meaningful results were the shear stress distribution which could be measured experimentally.

F. Experimental Procedure

Solution preparation

The total volume of the system was estimated to be 74 gallons. The weight of $K_4Fe(CN)_6$, $K_3Fe(CN)_6$, and KNO_3 for a concentration of 0.01, 0.01, and 1.0 normal, respectively, were added to the system. However, the $K_4Fe(CN)_6$ used probably absorbed some water during storage and its concentration turned out to be 0.0045N instead of 0.01N. The concentration of $K_3Fe(CN)_6$ came out to be 0.0093N and KNO_3 was 0.590N. Distilled water was used to fill the system, and then the system was pumped at a slow rate. At the same time pure nitrogen gas was bubbling through the solution in the reservoir to saturate the solution with nitrogen gas and to expel the dissolved oxygen (Dissolved oxygen reacts at the cathode in the same potential range as that of the ferricyanide ions.). This was continued for a few weeks. At the initial filling, bubbles were trapped in the horizontal section of the tunnel. They were removed by applying a vacuum at the reservoir. The pressure in the system was then reduced slowly. At one point the pressure on top of the horizontal section was at atmospheric pressure. The portholes on the tunnel were removed; a suction needle was introduced into the system to take away all the trapped air bubbles; the portholes were replaced; the vacuum was released. In

this way the system was made bubble free.

Preparation of Electrodes

First, the platinum surface was highly polished. The last polishing was done with a one-micron diamond paste. The electrodes were carefully washed by alcohol, and then they were cathodically treated in NaOH and rinsed thoroughly with distilled water. Next, the electrode was placed in the "side arm" where the electrode entered the system. The Lawrence Radiation Laboratory Wilson seal was placed in position. A bottle of the solution similar to the one in the system was used to fill the empty tube where now the cylinder was. The ball valve was slowly opened. This is crucial since trapped gas could be present on the cylinder side of the tube. The cylinder was then pushed into the channel and properly situated across the channel. The "O" ring at the end of the cylinder sealed off the porthole, separating the solution in the side arm from the solution in mark on the opposite end of the electrode. The leads of the electrode were then connected as described in the electrical circuit section earliar.

Current Measurement

Once the object was in position, it was left there without passing any current for a minimum of two hours. The flow rate and temperature of the system were carefully maintained at steady state. A potential of 600 mV was then applied between the electrodes. The output voltage from the amplifier was suppressed to less than 100 mV and was recorded on the t,Y-recorder. The amount of voltage suppressed was also recorded on the chart. To ascertain that the system was at steady state, in terms of

temperature, flow rate, and current, the potential was maintained for at least 1 hr. In some instances test runs were made by passing the current for 24 hours. A steady current was always observed when a constant temperature was maintained. Whenever there was a temperature fluctuation of more than 0.05°C, a drift in output voltage could be observed.

The position of the small electrode was changed and again no current was passed for at least two hours. In this manner, we were certain that the flow disturbance caused by the rotation of the electrode had completely died out. The same potential was imposed again, and the procedure was repeated for another position.

The same procedure was used for the shear stress measurement experiment.

To obtain the total current to the small electrodes, one only needs to apply Ohm's law,

$$I = \frac{V}{R} \tag{91}$$

where $R = 100{,}000\ \Omega$

V = total voltage

The surface areas of these electrodes were obtained by taking photographs under a microscope. The magnification used was 1 to 60. The photographs were matched and the area was measured by a polar planimeter. The areas for the electrode on the lucite cylinder and the 2-electrode cylinder were 1.699×10^{-2} cm^2 and 1.650×10^{-2} cm^2, respectively.

Measurement of Physical Properties

The density of the solution at 24° ± 0.01°C was measured with a pycnometer. The viscosity of the solution at the same temperature was measured by a viscometer. The diffusion coefficient was measured by means of a rotating disk. The apparatus and procedure were discribed in reference 8. The result is shown in Figure 22. The concentrations of the ferricyanide and ferrocyanide ions were determined by wet titration. $Fe(CN)_6^{-3}$ was by KI and $Na_2 S_2 O_3$ method, and $Fe(CN)_6^{-4}$ was by titration against $KMnO_4$ [34]. KNO_3 was determined by weighing. 100 ml of solution was extracted out and dried at room temperature by a applying a slight vacuum. The weight of the crystals was determined and the contribution due to potassium ferricyanide and potassium ferrocyanide was subtracted. The results of these properties are:

density = 1.01509 gm/c.c. at 24. ± 0.01°C

viscosity = 0.89092 Cp at 24.0 ± 0.01°C

diffusivity = $4.956 \times 10^{-6} cm^2/sec$ at 24.0 ± 0.01°C

concentration of $Fe(CN)_6^{-3}$ = 0.0093 N

$Fe(CN)_6^{-4}$ = 0.0045 N

KNO_3 = 0.590 N

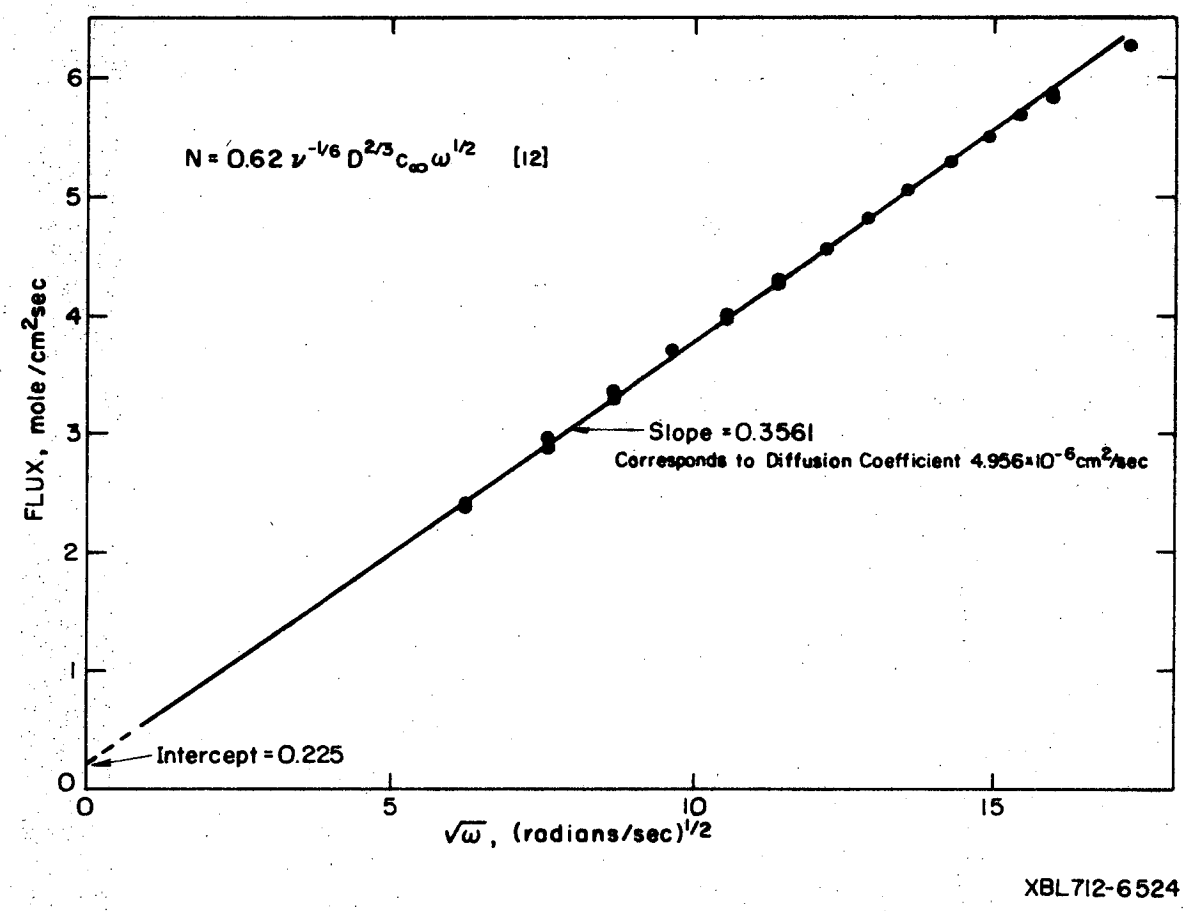

Fig. 22. Diffusivity measurement by rotating disk method.

CHAPTER VI: RESULTS AND DISCUSSION

Many technical difficulties were encountered in this experiment, and our objective was never achieved. However, we were able to overcome a majority of the problems involved. The unresolved problem merits a separate research project, and it shall be discussed later.

First, as mentioned earlier, the construction of the two-electrode cylinder was very difficult. Many designs were tried and modifications were made until finally a workable and durable cylinder was obtained. Second, the oscillation in the fluid flow had to be eliminated. This was achieved by installing a damping section in the flow system, which was discussed in the flow system of Chapter V. Third, the flow system was a large piece of equipment. Maintaining a uniform temperature throughout the system presented a great challenge. This was achieved by the following arrangements.

1) The laboratory room, outside the insulated hood, was maintained at a relatively cool temperature, and acted as a heat sink. Some of the cool air was allowed to leak into the hood through the sliding hood doors. The temperature of the room was controlled within 22 to 23°C.

2) Inside the hood two 60 watt light bulbs were connected to a relay system controlled by a Beckman thermometer. Also, there were two fans in the hood to maintain a thorough and fast circulation of the air inside. Temperature variation in the hood was, thus, in the order of ± 0.01°C.

3) The flow tunnel was covered by an open end box. It acted as a buffer so that the tunnel would not come in contact with any of the heated or cooled air at any time.

4) The cooling water to the heat exchanger was pumped from a constant temperature bath with a temperature fluctuation in the range of ± 0.01°C.

5) The motor assembly was enclosed in an insulated box. Compressed air was introduced from one end while a vacuum line at the opposite end pulled the air out. Thus, heat generated by the motor was quickly removed. But this proved to be insufficient since the air temperature varied day in and day out. Finally, the air supply was cooled to a steady temperature with the tap water discharged from the constant temperature bath.

With all these precautions the fluid temperature could be maintained within the limit of ±0.05°C indefinitely. It was at this point that we finally were able to obtain reproducible data.

The results were very discouraging as we found that natural convection due to the concentration difference was rather severe. Not at all like what Boeffard [9] had found. The results are shown in Figures 23 and 24.

Figure 23 shows the dimensionless surface shear stress distribution measured with the single electrode (on a lucite cylinder). Normally, without natural convection, the minimum should be at the front and rear stagnations. However, because of natural convection in the downward direction, the expected minimum at the front stagnation point was shifted to 110° at Re_t = 36.88. To confirm that this was caused by natural convection, the same measurements were made at zero flow rate. One could see the effect clearly and that the natural convection was symmetric along the vertical axis. Since no simple relationship exists between natural convection and forced convection, it is futile to try to back calculate the

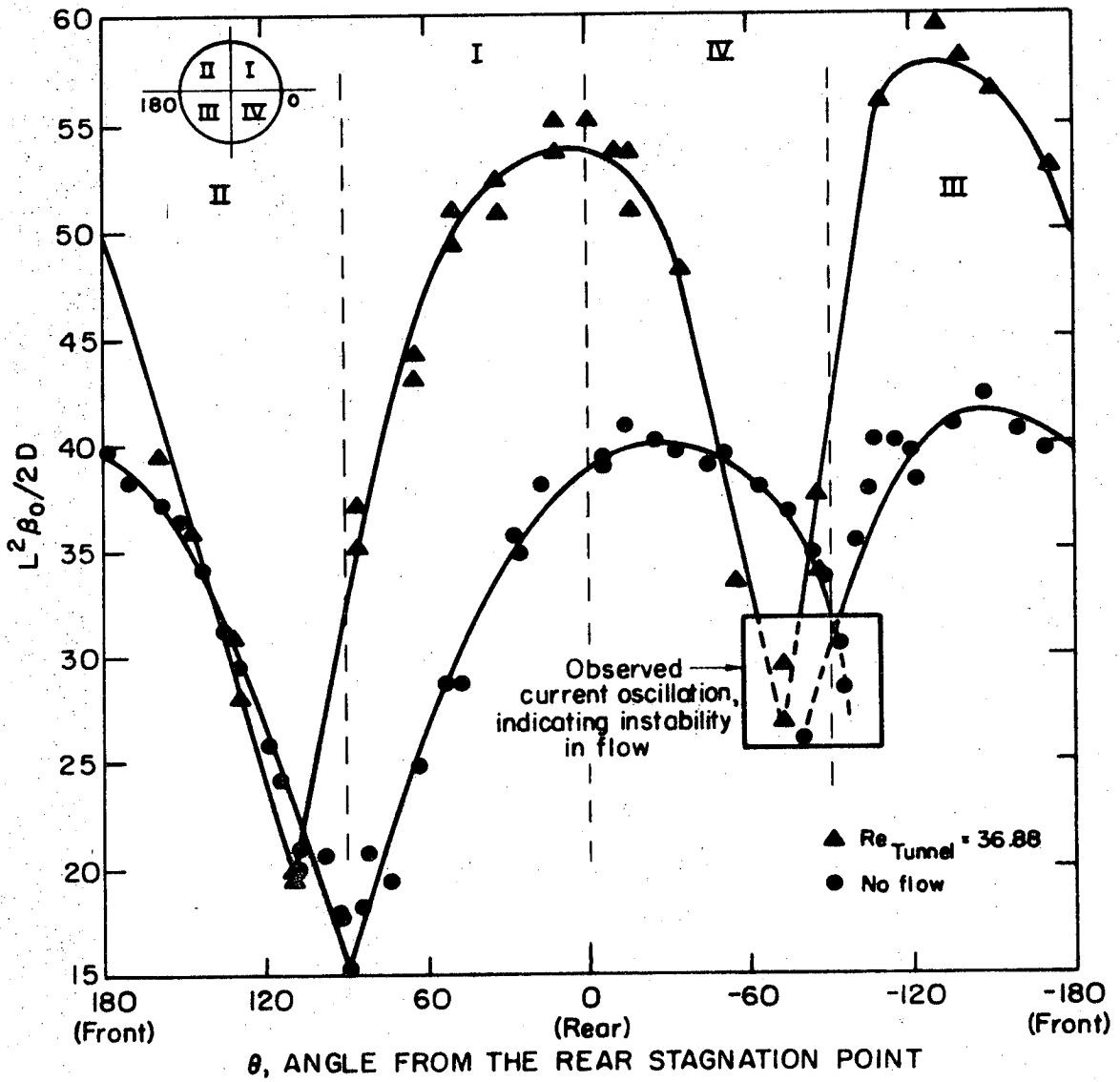

Fig. 23. Dimensionless surface shear stress distribution as measured by the single small electrode.

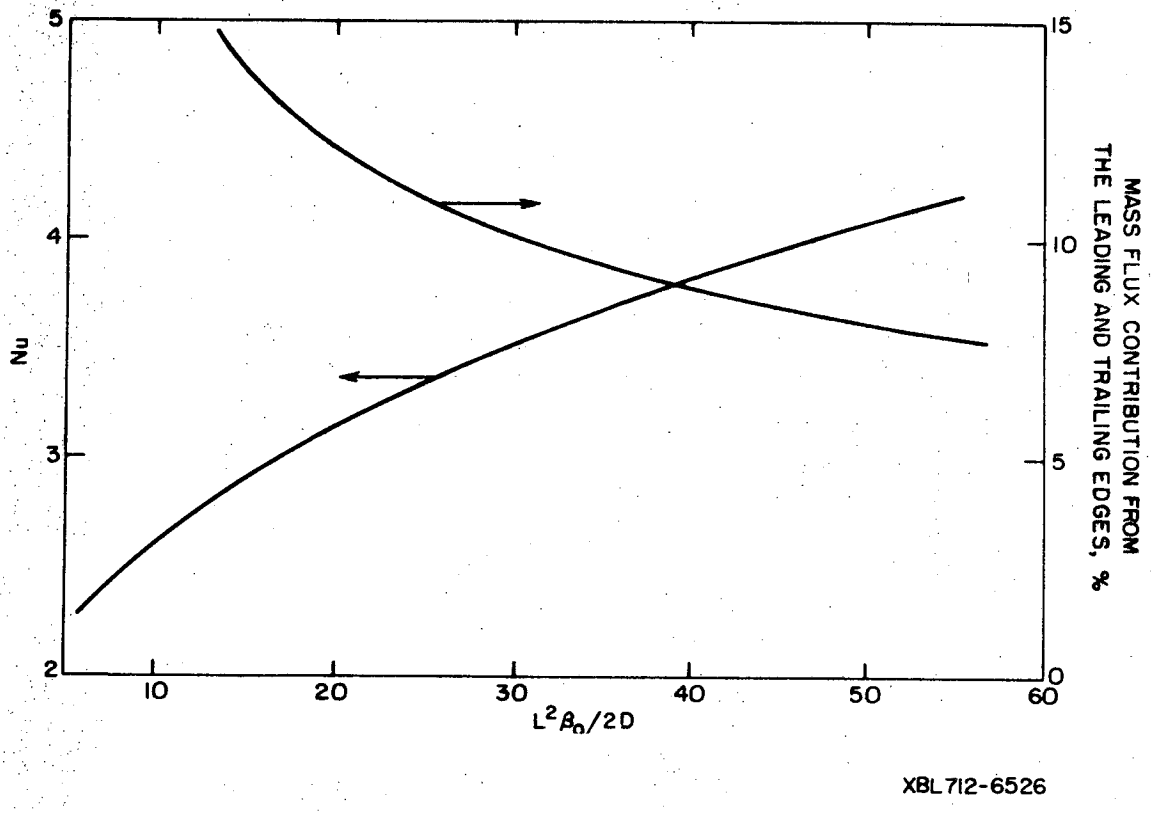

Fig. 24. Mass transfer to a flat plate according to equation (88) and its contribution from the leading and trailing edges.

forced convection contribution to the shear rates. In addition, the natural flow caused by the single electrode differed from that caused by the two-electrode system. Therefore, the shear rates measured did not correspond to the shear rates actually encountered in the mass transfer rate experiments, and could not be used to predict the mass transfer rates. However, as shown in Figure 24, the shear stress distribution experiment does illustrate the presence of the leading and trailing edge effects. Their contribution to the total mass flux was in the order of 10% for our particular experimental conditions.

To demonstrate that the system is operational, Figure 25 shows the mass flux to the small electrode on the two-electrode cylinder. It reflected the combined effect of forced and natural convections. The downward flow caused by natural convection forced the front stagnation point above the horizontal axis.

Although we did not achieve what we set out to do, we were satisfied that now we have a system which could provide a very slow, steady, and constant temperature flow. Work must be renewed to search for a system where the density change due to the concentration change in negligible. Incidentally, this may prove to be quite a challenge. Selman and Newman [35], recently made a theoretical investigation on the effect of supporting electrolyte on free convection. They found for $K_4Fe(CN)_6$, $K_3Fe(CN)_6$, and NaOH, the flow near the electrode and the flow away from the electrode could be in opposite directions. Regardless of these complications, we still believe that a suitable concentration combination can be found experimentally for the system used here. This can be accomplished by constructing a small constant temperature unit and using the single

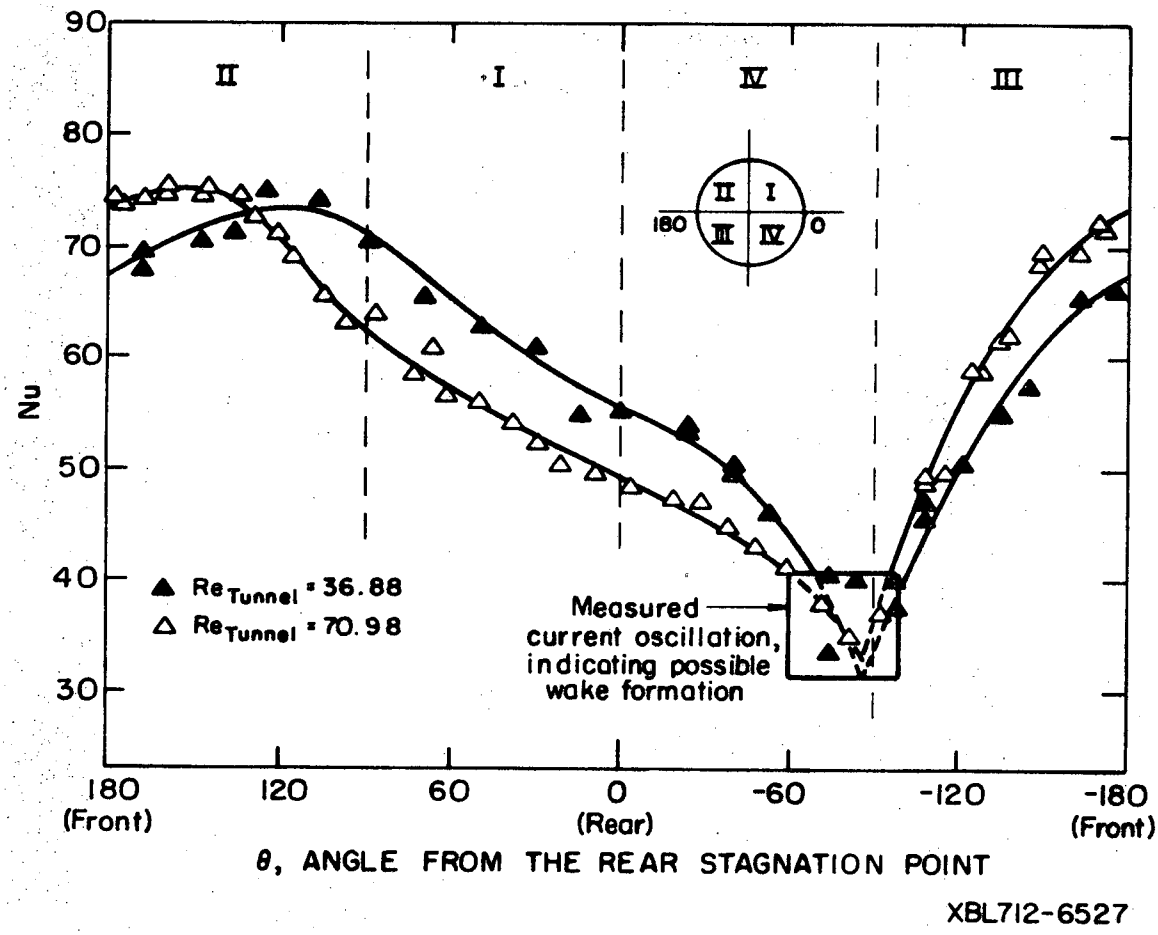

Fig. 25. Experimental mass transfer rates to a circular cylinder in a rectangular tunnel.

electrode cylinder to test the effect of natural convection of prepared solutions.

ACKNOWLEDGMENTS

The author would like to thank Mr. Philip E. Eggers for his help in setting up the electronics equipment and Mr. Julien A. Patenaude for his unwavering confidence and patience in constructing the electrodes. And mostly, my gratitude is due to Professor John Newman for his inspiration and guidance throughout this project.

This work was done under the auspices of the United States Atomic Energy Commission.

APPENDIX A.

Derivation for region 3.

The stream function for Stokes flow past a sphere is

$$\psi(r,\theta) = \left(\frac{A}{r} + Br - \frac{1}{2}\nu_\infty r^2\right)\sin^2\theta$$

$$= \left(-\frac{1}{4}\frac{\nu_\infty R^3}{r} + \frac{3}{4}\nu_\infty Rr - \frac{1}{2}\nu_\infty r^2\right)\sin^2\theta$$

$$= \nu_\infty R^2\left(-\frac{1}{4}\frac{R}{r} + \frac{3}{4}\frac{r}{R} - \frac{1}{2}\frac{r^2}{R^2}\right)\sin^2\theta. \qquad A(1)$$

Let us redefine a stream function variable appropriate to region 3.

$$\Psi = \frac{S^2}{3^{(5/3)}\pi^{(2/3)}}\left(\frac{1}{r^*} - 3r^* + 2r^{*2}\right) \qquad A(2)$$

where $S = \theta/\varepsilon$, $r^* = r/R$, $\varepsilon = (Pe/2)^{-(1/3)}$.

The solution in region 3 should match the boundary-layer solution as $r^* \to 1$. Then

$$\Psi \to \frac{S^2}{3^{(5/3)}\pi^{(2/3)}}\left(\frac{1}{1+r^*-1} - 3(1+r^*-1) + 2(1+r^*-1)^2\right)$$

$$\approx \frac{\theta^2}{3^{(5/3)}\pi^{(2/3)}\varepsilon^2}\left(1 - (r^*-1) + (r^*-1)^2 + O(r^*-1)^3 - 3 - 3(r^*-1)\right.$$

$$\left. + 2 + 4(r^*-1) + 2(r^*-1)^2\right)$$

$$= \frac{\theta^2}{3^{(5/3)}\pi^{(2/3)}\varepsilon^2}\left(3(r^*-1)^2 + O(r^*-1)^3\right)$$

$$\rightarrow \frac{\theta^2(r^*-1)^2}{3(2/3)_\pi(2/3)_\varepsilon 2} \quad . \qquad A(3)$$

The boundary-layer solution is

$$\Theta(\eta) = \frac{1}{\Gamma(4/3)} \int_0^\eta e^{-x^3}\, dx, \qquad A(4)$$

where $\eta = Y/g(\theta)$, $Y = (r^*-1)/\varepsilon$, $\qquad A(5)$

$$g(\theta) = \left(\frac{\pi - \theta + \frac{1}{2}\sin 2\theta}{\frac{1}{3}\sin^3\theta} \right)^{\frac{1}{3}} \quad . \qquad A(6)$$

This is supposed to match region 3 as $\theta \rightarrow 0$. Then

$$g \rightarrow \frac{\pi(1/3)_3(1/3)}{\theta} \text{ and } \eta = \frac{\theta(r^*-1)}{\pi(1/3)_3(1/3)_\varepsilon} \quad . \qquad A(7)$$

Thus in the region of matching,

$$\eta = \sqrt{\Psi} \quad . \qquad A(8)$$

Hence the solution in region 3 is

$$\Theta(\Psi) = \frac{1}{\Gamma(4/3)} \int_0^{\sqrt{\Psi}} e^{-x^3}\, dx \qquad A(9)$$

where Ψ is given by Equation A-(2).

For matching with region 4 one takes the limit of Equation A(9) as $S \to 0$ or $\Psi \to 0$.

$$\Theta \to \frac{\epsilon^{(1/2)}}{\Gamma(4/3)} \quad \frac{\theta/\epsilon^{3/2}}{3^{5/6}\pi^{1/3}} \left(\frac{1}{r^*} - 3r^* + 2r^{*2} \right)$$

APPENDIX B.

Construction of the Platinum Tube

The way the platinum tube was made may be of interest to some people, since it was rather straight forward and yet precise. A sheet of 0.010" thick platinum was joined by welding and it approximately fitted over a 0.480" drill blind, a steel rod of very precise dimension. The welded platinum tube, about 6" long, was placed over the drill blind and the two then hammered at high speed in a swage machine. The dye in the swage was set at 0.500". The end result was a completely smooth, and sealed platinum tube. 4" of this tube was cut off with a lathe, and used as the platinum cylinder electrode in the 2-electrode cylinder.

APPENDIX C.

Design of the Damping Section

The damping section was designed based on the following model.

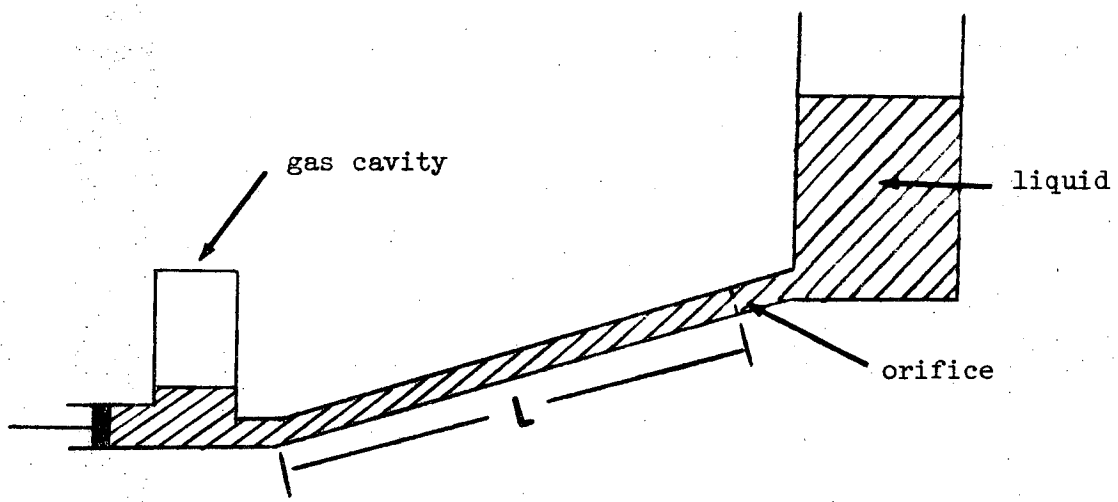

where a piston generated a wave, a gas cavity stored energy from the wave, and an orifice provided the resistance for the flow and to damp out the oscillation.

Newman studied such a system, seeking for its resonance frequency. The work was done in Oak Ridge National Laboratory. Detail can be found in his report ORNL-CF-60-5-135, 1960.

By linearizing the equations involved, a simple expression describing the system was arrived at,

$$G(S) = \frac{1}{T^2S^2 + 2\zeta TS + 1} \qquad (C\text{-}1)$$

where

$$T^2 = \frac{LV_o\rho}{A_T P_o} \qquad \text{(C-2)}$$

$$\zeta = \frac{1}{4}\rho g(R_A + R_B) \quad \frac{V_o A_T}{P_o L \rho} \qquad \text{(C-3)}$$

$$S = j\omega \qquad \text{(C-4)}$$

and

V_o = volume of gas cavity when at rest

P_o = pressure of gas cavity when at rest

ρ = density of liquid

A_T = cross-sectional area of pipe

R_A = resistance due to friction of the pipe

R_B = resistance due to the orifice

g = gravitational constant.

$j = \sqrt{-1}$

ω = frequency of piston.

L = length of the pipe

R_A and R_B were considered as constants here, although they varied with flow rate.

For effective damping action, $|G(S)| < 1$. Based one these equations, with ω set at 1500 rpm, pipe diameter at 1", we determined that with a gas cavity of 5000 cm^3, a pipe length of 80 inches there was quite a margin in R_B. This allowed us to use a valve in place of the orifice so that we had the flexibility to change the valve position when we varied the pump speed.

NOMENCLATURE

v_∞ = bulk velocity

c_∞ = bulk concentration

c_o = surface concentration

Pe = Peclet number

$\underline{v}^*$ = dimensionless velocity in vector form

Θ = dimensionless concentration $(C_i - C_o)/(C_\infty - C_o)$

v_r^* = radial velocity component

v_θ^* = tangential velocity component

D = diffusivity

r^* = r/R the dimensionless radius

R = radius of a sphere or a circular cylinder

θ = angle

$y = r^* - 1$ distance normal to the surface

$\varepsilon = (Pe/2)^{-1/3}$

$Y = y/\varepsilon$ Stokes flow or

$Y = y(2A/3D)^{1/3}$ for axisymmetric objects or

$Y = y(A/D)^{1/3}$ for 2-dimensional symmetrical objects

η = similarity variable

$\Gamma(4/3)$ = the gamma function of 4/3

$S = \theta/\varepsilon$

Ψ = Equation 19

$s = S/\sqrt{\varepsilon}$

$\xi = S\sqrt{Y}$ for axisymmetric objects or

$\xi = X\sqrt{Y}$ for 2-dimensional symmetrical objects

$\zeta = s\sqrt{2r^*/3}$

$\chi = \theta/\epsilon^2$

$R = \epsilon r^*$

$\beta(x) = \left.\frac{\partial\sqrt{x}}{\partial y}\right|_{y=0}$

$P(x)$ = the normal distance of the surface from the axis of symmetry

A = a constant defined by Equation (46)

$\overline{\Theta}$ = dimensionless concentration as defined by Equation (51) for axisymmetric objects or

$\overline{\Theta}$ = dimensionless concentration as defined by Equation (63) for 2-dimensional symmetrical cylinders

F = defined by Equation 66 or

F = Faraday constant

T = defined by Equation (68)

G = defined by Equation (70)

I = current, ampere

z = the number of electrons transferred in the electro-chemical reaction

N = mass transfer rate to an electrode

REFERENCES

1. Ping H. Sih and John Newman, Mass Transfer to the Rear of a Sphere in Stokes Flow, Int. J. Heat & Mass Transfer, 10, 1749 (1967).
2. John Newman, Mass Transfer to the Rear of a Cylinder at High Schmidt Numbers, Ind. & Eng. Chemistry Fundamentals, 8, 553 (1969).
3. V. G. Levich, Physicochemical Hydrodynamics (Prentice-Hall, Englewood Cliff, New Jersey, 1962), Section 14.
4. A. Acrivos and J. D. Goddard, Asymptotic Expansions for Laminar, Force-Convection Heat and Mass Transfer. Part 1. Low Speed Flows, J. Fluid Mechanics, 23, 273 (1965).
5. F. H. Garner and R. B. Keey, Mass Transfer from Single Solid Spheres-I, Transfer at Low Reynolds Numbers, Chem. Eng. Sci., 9, 119 (1958).
6. Harry J. Dimopoulos (Ph.D. thesis), Univ. of Illinois, Urbana, Illinois, 1968.
7. M. Eisenberg, Studies of Rates of Solid Dissolution and of Electrode Reactions at Rotating Cylinder Bodies (Ph.D. thesis), U.C. Berkeley, Calif., 1953.
8. Friedrich G. K. Bauke, Dieter Landolt, and Charles W. Tobias, Rotating Disk System for the Study of Metal Deposition from Nonaqueous Solvents, UCRL-17957, 1968.
9. A. J. P. M. Boeffard, Ionic Mass Transfer by Free Convection in a Redox System (M.S. thesis), UCRL-16624, 1966.
10. L. P. Reiss and T. J. Hanratty, Measurement of Instantaneous Rates of Mass Transfer to a Small Sink on a Wall, A. I. Ch. E. J., 8, 245 (1962).

11. L. P. Reiss, and T. J. Hanratty, An Experimental Study of the Unsteady Nature of the Viscous Sublayer, A. I. Ch. E. J., 9, 154 (1963).

12. J. E. Mitchell and T. J. Hanratty, A Study of Turbulence at a Wall using an Electrochemical Wall Shear Stress Meter, J. Fluid Mechanics, 26, 199 (1966).

13. M. A. Levêque, Les Lois de la Transmission de Chaleur par Convection, Annales des Mines, Memoirs, ser. 12, 13, 201 - 299, 305 - 362, 381 - 415 (1928).

14. C. J. Apelt, Some Studies of Fluid Flow at Low Reynolds Numbers (Ph.D. thesis), University of Oxford, England, June 1957.

15. G. Allen and R. Southwell, Relaxation Methods Applied to Determine the Motion, in Two Dimensions, of a Viscous Fluid Past a Fixed Cylinder, Quar. J. Mech. and Applied Math., 8, 129 (1955).

16. A. Thom, The Flow Past Circular Cylinder at Low Speeds, Proc. Roy. Soc. (London), 141 A, 651 (1933).

17. Hideo Takami and Herbert B. Keller, Steady Two-Dimensional Viscous Flow of an Incompressible Fluid Past a Circular Cylinder, High-Speed Computing in Fluid Dynamics, The Physics of Fluids Supplement II, II - 51 (1969).

18. P. C. Jain and K. Sankara Raa, Numerical Solution of Unsteady Viscous Imcompressible Fluid Flow Past a Circular Cylinder, Ibid., II - 57 (1969).

19. S. C. R. Dennis and Gan-Zu Chang, Numerical Integration of the Navier-Stokes Equations for Steady Two-Dimension Flow, Ibid., II - 88 (1969).

20. Mitutosi Kawaguti, Numerical Solution of the Navier-Stokes Equations for the Flow Around a Circular Cylinder at Reynolds Number 40, J. Phys. Soc. Japan, 8, 747 (1953).

21. Thomas Atkins, Water Tunnel With Moving Walls (M.S. thesis), UCRL-16188, 1965.

22. A. Acrivos and T. D. Taylor, Heat and Mass Transfer from Single Spheres in Stokes Flow, Physics Fluids, 5, 387 (1962).

23. M. J. Lighthill, Proc, Roy. Soc. London, A202, 359 (1950).

24. A. Acrivos, Phys. Fluids, 3, 657 (1960)

25. V. G. Jenson, Proc. Roy. Soc. London, A249, 346 (1959).

26. A. E. Hamielec, T. W. Hoffman, and L. L. Ross, Numerical Solution of the Navier-Stokes Equation for Flow Past Spheres: Part I. Viscous Flow Around Spheres With and Without Radial Mass Efflux, A. I. Ch. E. J., Vol. 13, 2, 212 (1967).

27. Ping H. Sih, Numerical Computation of Flow Past Obstacles (M.S. thesis), UCRL-16653, 1966.

28. Southwell and Squire, A Modification of Oseen's Approximate Equation for the Motion in Two Dimensions of a Viscous Incompressible Fluid, Phil. Trans. Roy. Soc. London, A232, 27 (1933).

29. B. H. Lamb, Hydrodynamics (New York, 1945).

30. John Newman, The Fundamental Principles of Current Distribution and Mass Transport in Electrochemical Cells in Electroanalytical Chemistry, edited by Allen J. Bard (Marcel Dekker, Inc., New York, to be published). UCRL-20547.

31. John Newman, The Graetz Problem, UCRL-18646, 1969.

32. William H. Smyrl and John Newman, Limiting Current on a Rotating Disk with Radial Diffusion, UCRL-20378, Nov. 1970.

33. L. S. Han, Hydrodynamic Entrance Lengths for Incompressible Laminar Flow in Rectangular Ducts, J. Applied Mechanics, Transactions of ASME, 403 (1960).

34. Francis Sutton and Julius Grant, A Systematic Handbook of Volumetric Analysis (Butterworths Scientific Publications, London, 1955).

35. J. R. Selman and John Newman, Free Convection Mass Transfer with a Supporting Electrolyte, UCRL-20306, 1970.

LEGAL NOTICE

This report was prepared as an account of work sponsored by the United States Government. Neither the United States nor the United States Atomic Energy Commission, nor any of their employees, nor any of their contractors, subcontractors, or their employees, makes any warranty, express or implied, or assumes any legal liability or responsibility for the accuracy, completeness or usefulness of any information, apparatus, product or process disclosed, or represents that its use would not infringe privately owned rights.

TECHNICAL INFORMATION DIVISION
LAWRENCE RADIATION LABORATORY
UNIVERSITY OF CALIFORNIA
BERKELEY, CALIFORNIA 94720